THE JOURNAL OF PHYSICAL CHEMISTRY A
A JOURNAL OF THE AMERICAN CHEMICAL SOCIETY

pubs.acs.org/JPCA

Article

Nuclear Spin Relaxation in Cold Atom−Molecule Collisions

Published as part of The Journal of Physical Chemistry virtual special issue "Cold Chemistry".

Rebekah Hermsmeier, Xiaodong Xing, and Timur V. Tscherbul*

Cite This: *J. Phys. Chem. A* 2023, 127, 4511−4525

Read Online

ACCESS | Metrics & More | Article Recommendations

ABSTRACT: We explore the quantum dynamics of nuclear spin relaxation in cold collisions of $^1\Sigma^+$ molecules with structureless atoms in an external magnetic field. To this end, we develop a rigorous coupled-channel methodology, which accounts for rotational and nuclear spin degrees of freedom of $^1\Sigma^+$ molecules and their interaction with an external magnetic field as well as anisotropic atom−molecule interactions. We apply the methodology to study the collisional relaxation of the nuclear spin sublevels of ^{13}CO molecules immersed in a cold buffer gas of ^{4}He atoms. We find that nuclear spin relaxation in the ground rotational manifold ($N = 0$) of ^{13}CO occurs extremely slowly due to the absence of direct couplings between the nuclear spin sublevels. The rates of collisional transitions between the rotationally excited ($N = 1$) nuclear spin states of ^{13}CO are generally much higher due to the direct nuclear spin−rotation coupling between the states. These transitions obey selection rules, which depend on the values of space-fixed projections of rotational and nuclear spin angular momenta (M_N and M_I) for the initial and final molecular states. For some initial states, we also observe a strong magnetic field dependence, which can be understood by using the first Born approximation. We use our calculated nuclear spin relaxation rates to investigate the thermalization of a single nuclear spin state of ^{13}CO($N = 0$) immersed in a cold buffer gas of ^{4}He. The calculated nuclear spin relaxation times ($T_1 \simeq 1$ s at $T = 1$ K at a He density of 10^{-14} cm^{-3}) display a steep temperature dependence decreasing rapidly at elevated temperatures due to the increased population of rotationally excited states, which undergo nuclear spin relaxation at a much faster rate. Thus, long relaxation times of $N = 0$ nuclear spin states in cold collisions with buffer gas atoms can be maintained only at sufficiently low temperatures ($k_BT \ll 2B_e$), where B_e is the rotational constant.

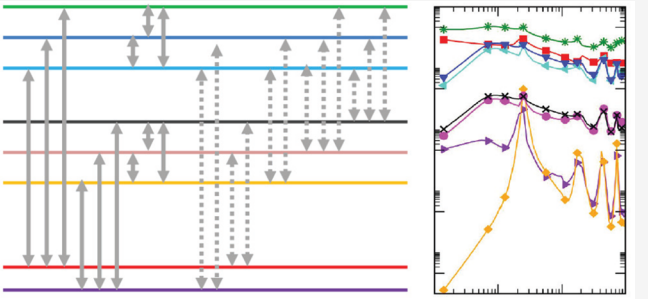

1. INTRODUCTION

Cold and ultracold molecular gases prepared in single rovibrational and spin quantum states can be efficiently controlled with external electromagnetic fields,[1,2] thereby forming a unique platform for exploring fundamental concepts of gas-phase reaction dynamics such as long-lived complex formation, universal dynamics, external field control, and the role of quantum chaos in chemical reactivity.[3−5] Ultracold polar molecules also hold promise for quantum information science, precision spectroscopy, and searches for new physics beyond the standard model.[1,5,6] The experimental realization of these proposals demands dense, cold, and long-lived molecular ensembles. As such, understanding low-temperature collisions within these ensembles, which limit both the maximum achievable density and lifetime, has long been a major thrust in the field.[3−5]

Atom−molecule and molecule−molecule collisions can have beneficial as well as detrimental effects on the stability of cold molecular gases. While elastic collisions are a main driving force behind sympathetic and evaporative cooling,[1,7,8] inelastic collisions lead to heating and/or trap loss. In particular, inelastic collisions can flip the orientation of molecular electron spins, leading to spin relaxation (also known as spin depolarization).[8−10] As collisional spin relaxation is a primary loss mechanism for magnetically trapped molecules, it has been the subject of much experimental and theoretical work (e.g., refs 8−20 and references therein). Volpi and Bohn[9] and Krems and Dalgarno[10] performed the first rigorous coupled-channel calculations of cold collisions between open-shell molecules and atoms in the presence of an external magnetic field. This work has since been extended to a variety of ultracold atom−molecule and molecule−molecule systems and has generated theoretical predictions of their low-temperature collisional properties.[8,18−21]

Received: December 9, 2022
Revised: April 24, 2023
Published: May 16, 2023

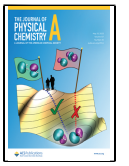

By comparison, collisional relaxation of nuclear spins has drawn much less attention. Nuclear spin-flipping collisions are responsible for the stability of the nuclear spin states of molecules immersed in a cold inert buffer gas (such as He or Ne). These systems can be realized experimentally using cryogenic buffer gas cooling,[11,22−34] and they are interesting for a variety of reasons. First, preparing molecules in a single nuclear spin (or hyperfine) state enhances the sensitivity of spectroscopic measurements[25−34] and is essential for the initialization steps of molecule-based quantum information processing protocols. One example is hyperpolarized nuclear magnetic resonance (NMR), which relies on driving populations of nuclear spin states out of thermal equilibrium as a means to enhance the sensitivity of conventional (thermal) NMR.[35−38] Because nuclear spins interact weakly with their environment, they could be an ideal platform for long-term quantum information storage.[39,40] Our ability to use buffer-gas-cooled molecules for these applications is currently hindered by the lack of knowledge of collisional nuclear spin relaxation rates. Indeed, if these rates turn out to be large, then collisional thermalization would lead to rapid decoherence of the nuclear spin superposition states, making them unsuitable for quantum information processing.

Nuclear spins can affect molecular collisions and chemical reactions through several mechanisms. First, nuclear spin statistics restrict the number of available reactants and/or product states. As a prime example, only odd partial waves are allowed for collisions of identical Fermions in the same internal states, leading to a suppression of the ultracold chemical reaction KRb + KRb → K_2 + Rb_2.[41,42] Homonuclear diatomic molecules can exist in the form of different nuclear spin isomers, such as ortho- and para-H_2, which can exhibit dramatically different chemical reactivity at ultralow temperatures, as seen in theoretical calculations.[4,43] Nuclear spin isomers of polyatomic molecules such as methylene (CH_2) have been predicted to have markedly different spin relaxation rates in cold collisions with He atoms,[44] and ortho- and para-water molecules have different reactivity toward trapped diazenylium ions.[45] Second, because nuclear spins are weakly coupled to the other degrees of freedom, it is expected that the total nuclear spin of the collision complex should be conserved, which leads to nuclear spin selection rules.[46] These selection rules have recently been observed experimentally for the ultracold chemical reaction KRb + KRb → K_2 + Rb_2, which populates only even (odd) rotational states of K_2 (Rb_2)[47] when the reactants are prepared in single, well-defined nuclear spin states. Finally, hyperfine interactions between the nuclear spins and the other degrees of freedom (such as the electron spins in open-shell atoms and molecules) play a crucial role in low-temperature atomic and molecular collisions,[48−52] being largely responsible for the occurrence of magnetic Feshbach resonances in ultracold atom−atom collisions.[53] However, rigorous theoretical studies of nuclear spin effects in ultracold molecular collisions have been largely limited to hyperfine interactions in open-shell molecule−atom collisions.[7,49,50] Queménér et al. recently proposed a simple state decomposition model[54] to describe the effects of nuclear spin conservation and external magnetic fields on the product state distributions of the ultracold chemical reaction KRb + KRb → K_2 + Rb_2. While the model describes these effects remarkably well, it makes a number of assumptions, such as neglecting the rotational structure of the reactants and products. Model calculations on ultracold RbCs + RbCs,[55] Li + CaH,[51] and Na + NaLi collisions[52] used severely limited basis sets, which did not produce converged results when hyperfine degrees of freedom were included.

Here, we develop a rigorous quantum mechanical theory of nuclear spin relaxation in collisions of $^1\Sigma^+$molecules with structureless atoms in the presence of an external magnetic field. We apply the theory to calculate numerically converged cross sections and rate coefficients for transitions between the different rotational and nuclear spin sublevels of ^{13}CO molecules in low-temperature collisions with ^{4}He atoms and to explore their dependence on the collision energy and magnetic field. Our calculations show that such transitions follow distinct selection rules. For example, nuclear spin-flipping transitions occur very slowly in the ground rotational state manifold, leading to nuclear spin relaxation (T_1) times on the order of 1 s at a buffer-gas density of 10^{-14} cm^{-3} and T = 1 K. The long relaxation times of the nuclear spin sublevels of the ground rotational state imply their potential utility for precision spectroscopy and quantum information storage. The long T_1 times are maintained as long as the buffer gas temperature is much lower than the spacing between the ground and the first excited rotational levels.

The rest of this article is structured as follows. In Section 2, we present the quantum scattering methodology for atom−molecule collisions in a magnetic field, which explicitly includes the nuclear spin degrees of freedom of $^1\Sigma^+$ molecules. We then apply the methodology to obtain converged cross sections for nuclear spin transitions in cold He + CO collisions. The relevant computational details are given at the end of Section 2. In Section 3, we present and analyze the cross sections and rate constants for nuclear spin relaxation in cold He + CO collisions. In Section 3.4, we consider the dynamics of nuclear spin sublevels of CO molecules immersed in a cold buffer gas of He. Section 4 summarizes the main results of this work.

2. THEORY

In this section, we will develop the quantum theory of collisions between $^1\Sigma^+$ molecules bearing a single nuclear spin (such as $^{13}C^{16}O$) and structureless S-state atoms in an external magnetic field. We will next apply the theory to calculate the cross sections and rates for nuclear-spin-changing transitions in cold ^{4}He + $^{13}C^{16}O(^1\Sigma^+)$ collisions.

The Hamiltonian of the atom−molecule collision complex may be written as

$$\hat{H} = -\frac{1}{2\mu R}\frac{\partial^2}{\partial R^2}R + \frac{\hat{L}^2}{2\mu R^2} + \hat{V}(R, r, \theta) + \hat{H}_{\mathrm{mol}} \quad (1)$$

where the orbital angular momentum operator $\hat{L}$ describes the orbital motion of the colliding particles, $\mu = M_{\mathrm{at}}M_{\mathrm{mol}}/(M_{\mathrm{at}} + M_{\mathrm{mol}})$ is the reduced mass of the complex, and $\hat{V}$ represents the atom−molecule interaction potential in Jacobi coordinates (R, r, θ), where $r = |\mathbf{r}|$ is the internuclear distance in the diatomic molecule, $R = |\mathbf{R}|$ is the separation vector from the atom to the center of mass of the molecule, and θ is the angle between $\mathbf{R}$ and $\mathbf{r}$. Here, we consider collisions of $^{13}C^{16}O$ molecules with structureless atoms (such as ^{4}He), and hence the atomic Hamiltonian can be omitted from eq 1. The interaction potential $V(R, r, \theta)$ approaches zero as $R \to \infty$.

The effective Hamiltonian of the $^1\Sigma^+$ molecule in its ground electronic and vibrational states[56,57]

https://doi.org/10.1021/acs.jpca.2c08646
J. Phys. Chem. A 2023, 127, 4511−4525

$$\hat{H}_{\mathrm{mol}} = \hat{H}_{\mathrm{rot}} + \hat{H}_{\mathrm{hf}} + \hat{H}_{\mathrm{Z}} \tag{2}$$

can be decomposed into the rotational, hyperfine, and Zeeman terms

$$\hat{H}_{\mathrm{rot}} = B_e\hat{\mathbf{N}}^2 - D_v\hat{\mathbf{N}}^4$$
$$\hat{H}_{\mathrm{hf}} = A\hat{\mathbf{I}}\cdot\hat{\mathbf{N}}$$
$$\hat{H}_Z = -g_N\mu_N\hat{N}_zB - g_I\mu_N\hat{I}_zB - \frac{1}{\sqrt{6}}B^2\sum_q {D_{0q}}^{2*}(\omega)\hat{T}_q^{\,2}(\chi) \tag{3}$$

where B_e is the rotational constant, D_v is the centrifugal distortion constant, $\hat{\mathbf{N}}$ is the rotational angular momentum operator, $\hat{\mathbf{I}}$ is the nuclear spin operator, A is the nuclear spin−rotation interaction constant, g_N is the rotational g factor, g_I is the nuclear g factor, μ_N is the nuclear magneton, B is the magnetic field, ${D_{0q}}^2(\omega)$ is a Wigner D function of the Euler angles ω, which determine the position of the molecular axis in the space-fixed frame, and $\hat{T}_q^{\,2}(\chi)$ is the magnetic susceptibility tensor.[57]

The hyperfine structure of ^{13}CO arises from the nuclear spin of ^{13}C (I = 1/2) and includes the nuclear spin−rotation interaction defined by $\hat{H}_{\mathrm{hf}}$ in eq 3. The Zeeman term $\hat{H}_Z$ accounts for the interaction of the external magnetic field with the molecular rotational angular momentum, nuclear spin, and diamagnetic susceptibility[58] represented by the first, second, and third terms, respectively, in the third line of eq 3.

We assume that the external magnetic field B is directed along the space-fixed (SF) quantization axis, z. The Hamiltonian in eq 3 employs the rigid rotor approximation with a correction for centrifugal distortion. This effectively neglects the vibrational motion of the molecule, which is known to be a good approximation for collisions with weakly perturbing buffer gas atoms (such as ^{4}He) at low temperatures.[4,58]

To solve the quantum scattering problem for the atom−molecule collision system, we expand the total wave function of the system in a complete set of uncoupled basis functions in the SF frame

$$|\Psi\rangle = \frac{1}{R}\sum_{N,M_N}\sum_{M_I}\sum_{L,M_L} F^M_{NM_NIM_ILM_L}(R)|NM_N\rangle|IM_I\rangle|LM_L\rangle \tag{4}$$

where M_N, M_I, and M_L indicate the projections of $\hat{\mathbf{N}}$, $\hat{\mathbf{I}}$ and $\hat{\mathbf{L}}$ onto the SF z axis. The basis set used in eq 4 is similar to the one used in the previous work of Volpi and Bohn[9] and Krems and Dalgarno[10] for open-shell $^2\Sigma$ and $^3\Sigma$ molecules colliding with structureless atoms. The only difference is that our basis functions $|IM_I\rangle$ describe the nuclear spin degrees of freedom in $^1\Sigma$ molecules rather than the electron spins of $^2\Sigma$ and $^3\Sigma$ molecules.

The projection of the total angular momentum $M = M_N + M_I + M_L$, unlike the total angular momentum itself, is conserved for collisions in a magnetic field. Substituting eq 4 into the time-independent Schrödinger equation, $\hat{H}|\Psi\rangle = E|\Psi\rangle$, where E is the total energy, we obtain a system of coupled-channel (CC) equations for the expansion coefficients $F^M_{NM_NIM_ILM_L}$ (omitting the initial quantum numbers N_i, M_{N_i}, I_i, M_{I_i}, L_i, and M_{L_i} for simplicity)

$$\left[\frac{\mathrm{d}^2}{\mathrm{d}R^2} + 2\mu E - \frac{L(L+1)}{R^2}\right]F^M_{NM_NIM_ILM_L}(R) = 2\mu\sum_{N',M_N'}\sum_{M_I'}\sum_{L',M_L'}\langle NM_NIM_ILM_L|\hat{V} + \hat{H}_{\mathrm{mol}}|N'M_N'I'M_I'L'M_L'\rangle F^M_{N'M_N'IM_I'L'M_L'}(R) \tag{5}$$

where the summation is carried out over all of the channels included in the basis set. The CC values in eq 5 are parametrized by the matrix elements of the molecular Hamiltonian and of the interaction potential in the direct-product basis (eq 4). Below we describe the evaluation of these matrix elements.

We begin with the matrix elements of the Hamiltonian of an isolated $^1\Sigma$ molecule (eq 3). Because the rotational Hamiltonian is independent of the nuclear spin and orbital degrees of freedom, it is diagonal in M_I, L, and M_L:

$$\langle NM_NIM_ILM_L|\hat{H}_{\mathrm{rot}}|N'M_N'IM_I'L'M_L'\rangle = \delta_{N,N'}\delta_{M_N,M_N'}\delta_{M_I,M_I'}\delta_{L,L'}\delta_{M_L,M_L'}[B_eN(N+1) - D_vN^2(N+1)^2] \tag{6}$$

The matrix elements of the hyperfine Hamiltonian $\hat{H}_{\mathrm{hf}}$ are obtained by expanding the spin−rotation interaction $A\hat{\mathbf{I}}\cdot\hat{\mathbf{N}}$ in terms of the raising and lowering operators $\hat{I}_\pm$ and $\hat{N}_\pm$[59]

$$\langle NM_NIM_ILM_L|\hat{H}_{\mathrm{hf}}|N'M_N'I'M_I'L'M_L'\rangle = \delta_{L,L'}\delta_{M_L,M_L'}A\Big[\delta_{M_N,M_N'}\delta_{M_I,M_I'}M_N'M_I' + \frac{1}{2}(C_+^{I,M_I'}C_-^{N,M_N'}\delta_{M_I,M_I'+1}\delta_{M_N,M_N'-1} + C_-^{I,M_I'}C_+^{N,M_N'}\delta_{M_I,M_I'-1}\delta_{M_N,M_N'+1})\Big] \tag{7}$$

where $C_\pm^{j,m} = \sqrt{j(j+1) - m(m\pm1)}$. The matrix elements of the Zeeman interaction are diagonal in the uncoupled basis since the basis states $|IM_I\rangle$ are eigenstates of $\hat{I}^2$ and $\hat{I}_z$

$$\langle NM_NIM_ILM_L|\hat{H}_Z|N'M_N'IM_I'L'M_L'\rangle = \delta_{N,N'}\delta_{M_N,M_N'}\delta_{L,L'}\delta_{M_L,M_L'}\delta_{M_I,M_I'}(-g_N\mu_NM_NB - g_I\mu_NM_IB) - \delta_{N,N'}\delta_{M_N,M_N'}\delta_{L,L'}\delta_{M_L,M_L'}\delta_{M_I,M_I'}B^2 \times \frac{3{M_N}^2 - N(N+1)}{3(2N-1)(2N+3)}(\chi_{\parallel} - \chi_{\perp}) \tag{8}$$

where the matrix elements of the diamagnetic Zeeman interaction are proportional to the difference between $\chi_\parallel$ and $\chi_\perp$, the parallel and perpendicular components of the diamagnetic susceptibility tensor of CO (see eq (8.140) of ref 56.). Test calculations show that the diamagnetic Zeeman interaction becomes noticeable only at high magnetic fields (B > 1 T).

The atom−molecule interaction potential is rotationally invariant and independent of the nuclear spin. Hence, its matrix elements are diagonal in the total angular momentum projection M and in the nuclear spin projection M_I[10]

$$\langle NM_NIM_ILM_L|V(R,r,\theta)|N'M_N'I'M_I'L'M_L'\rangle = \delta_{M_I,M_I'}(-1)^{M_L'-M_N} \times [(2L+1)(2L'+1)]^{\frac{1}{2}}[(2N+1)(2N'+1)]^{\frac{1}{2}}\sum_\lambda V_\lambda(R)\begin{pmatrix} L & \lambda & L' \\ 0 & 0 & 0\end{pmatrix} \times \begin{pmatrix} L & \lambda & L' \\ -M_L & M_L - M_L' & M_L'\end{pmatrix}\begin{pmatrix} N & \lambda & N' \\ 0 & 0 & 0\end{pmatrix}\begin{pmatrix} N & \lambda & N' \\ -M_N & M_N - M_{N'} & M_{N'}\end{pmatrix} \tag{9}$$

where the Legendre coefficients $V_\lambda(R)$ are obtained by expanding the interaction potential energy surface (PES) in

https://doi.org/10.1021/acs.jpca.2c08646
J. Phys. Chem. A 2023, 127, 4511−4525

Legendre polynomials $V(R, \theta) = \sum_\lambda V_\lambda(R)\ P_\lambda(\cos\theta)$ (see Section 2.1 for details).

To obtain the full state-to-state reactance (K) and scattering (S) matrices, we match the asymptotic solutions of CC eq 5 to the standard asymptotic form given by linear combinations of the Riccati-Bessel and Neumann functions at large R.[60]

The state-to-state scattering cross sections are related to the S matrix elements at a given collision energy E

$$\sigma_{\gamma\to\gamma'}(E) = \frac{\pi}{k_\gamma^2}\sum_M\sum_{LM_L}\sum_{L'M_L'}|\delta_{LM_L,L'M_L'}\delta_{\gamma\gamma'} - S^M_{\gamma LM_L,\gamma' L'M_L'}|^2 \tag{10}$$

where γ and γ' refer to the eigenstates of the isolated molecule's Hamiltonian (eq 3) in the presence of a magnetic field, $|\gamma\rangle = \sum_{NM_NM_I} C_{\gamma,NM_NM_I}(\mathrm{B})|NM_N\rangle|IM_I\rangle$, and $k_\gamma = (2\mu E)^{1/2}$ is the collision wavevector. The matrix of solutions of CC equations is transformed to the eigenstate basis before the application of scattering boundary conditions.[10]

The thermal state-to-state rate coefficients at temperature T are obtained by averaging the cross sections over the Maxwell–Boltzmann velocity distribution[61]

$$K_{\gamma\to\gamma'}(T) = \left(\frac{8}{\pi\mu k_B^3 T^3}\right)^{1/2}\int_0^\infty \sigma_{\gamma\to\gamma'}(E)E\exp\left(-\frac{E}{k_BT}\right)\mathrm{d}E \tag{11}$$

where k_B is the Boltzmann constant and T is the temperature.

2.1. Computational Details. We use the following spectroscopic constants of $^{13}C^{16}O$ to parametrize the Hamiltonian in eq 3: B_e = 55.101 GHz,[62] $D_v = 1.676\times10^{-4}$ GHz,[62] $A = 3.27\times10^{-5}$ GHz,[57] $g_N = -0.2595$,[57] $g_I = 1.40482$,[63] and the diamagnetic susceptibility anisotropy $(\chi_\parallel - \chi_\perp) = -6.85829\times10^{-14}$ cm^{-1}/T^2.[57]

We use the log-derivative approach[60,64] to numerically integrate the CC (eq 5) for He + $^{13}C^{16}O$ collisions on a radial grid from R_{min} = 3.0 a_0 to R_{max} = 110.0 a_0 with a constant grid step of 0.02 a_0). While here we are interested only in transitions between the Zeeman states in the first two rotational manifolds (N = 0 and 1), the CC basis must include closed channels to ensure numerical convergence of the calculated cross sections. We found that it is necessary to include the 11 lowest rotational states of CO in our calculations. For collision energies below (above) 2 K, we include all partial waves with $L \le 10$ ($L \le 13$), which results in a total of 288 (450) coupled channels.

To calculate collision rates, we averaged the calculated cross sections according to eq 11 on a grid of collision energies from 1.44×10^{-6} to 14.4 K with 102 grid points fitted with cubic splines. In doing so, we found that calculating the upward excitation rates (e.g., for the $|2\rangle \to |3\rangle$ transition) is challenging because excitation transitions are energetically forbidden at collision energies below the N = 1 threshold (5.3 K), and their cross sections increase sharply from zero to a finite value above the threshold. As this behavior is very hard to fit, we use the principle of detailed balance

$$\frac{k_{f\to i}(T)}{k_{i\to f}(T)} = e^{(E_f - E_i)/k_BT} \tag{12}$$

to obtain the desired excitation rates, where E_i and E_f are the energies of the initial and final molecular states involved in the transition.

We use an accurate *ab initio* PES for He-CO developed by Heijmen et al.[65] using a symmetry-adapted perturbation theory approach.[66] This PES was used in several quantum scattering calculations by Balakrishnan et al.[58] and by Wang et al.,[61] which focused on rovibrational transitions in $^{12}C^{16}O$ induced by ultracold collisions with He atoms. Low-energy scattering resonances in He + CO collisions were observed in a merged beam experiment and compared to theoretical calculations using several PESs.[67] We compare our results against the previous calculations[58,61] in Appendix B to test our He + CO scattering code. The He-CO PES is weakly anisotropic, with a single minimum of −23.734 cm^{-1} located at R = 6.53 a_0, θ = 48.4°, and r = 2.132 a_0 (the equilibrium bond length of CO). We expand the θ dependence of the PES in 12 Legendre polynomials.

The previous calculations did not account for the nuclear spin of the $^{13}C^{16}O$ isotopologue, which is the subject of interest here. Because the original He-CO PES was defined in the Jacobi coordinate system with its origin at the center of mass of $^{12}C^{16}O$, we need to rescale the PES to account for the shift of the center of mass. The rescaling procedure is described in Appendix C.

3. RESULTS AND DISCUSSION

In this section, we apply the theory developed above to study the nuclear spin dynamics in cold collisions of $^{13}C^{16}O$ molecules with ^{4}He atoms. We will present state-to-state scattering cross sections and collision rates for all initial Zeeman levels of $^{13}C^{16}O$ (N = 0, 1) in collisions with ^{4}He atoms. We also calculate the magnetic field dependence of inelastic collision rates and explain it using a simple model. Finally, we use the computed collision rates to explore the thermalization dynamics of a single nuclear spin state of $^{13}C^{16}O$ immersed in a cold buffer gas of ^{4}He, and we estimate the nuclear spin relaxation times.

3.1. Energy Levels of $^{13}C^{16}O$. Figure 1 displays the Zeeman levels of $^{13}C^{16}O$ as a function of the magnetic field. The electronic spin of $^{13}C^{16}O$ is zero, and the energy splittings are determined by an interplay between the hyperfine (spin–

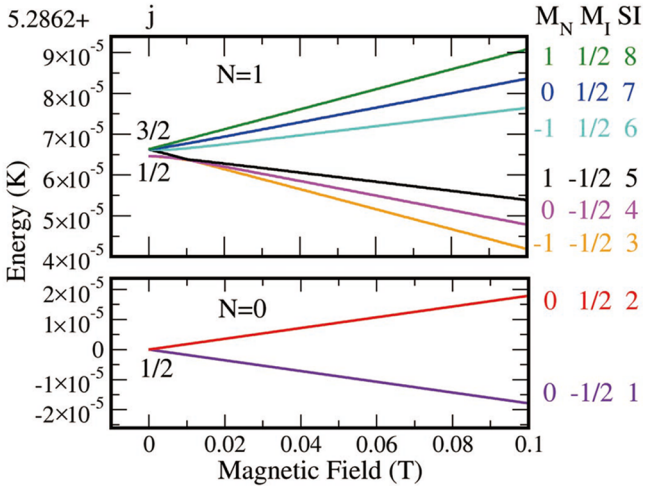

Figure 1. Zeeman energy levels of $^{13}C^{16}O$ as a function of the magnetic field. Each level is labeled by the quantum numbers j (in the low-field limit) and N, M_N, and M_I (in the high-field limit) and by its state index (SI). 1 K = 0.695 cm^{-1}. Top and bottom panels show the levels in rotational manifolds N = 1 and N = 0, respectively.

https://doi.org/10.1021/acs.jpca.2c08646
J. Phys. Chem. A 2023, 127, 4511−4525

rotation) interaction due to the nuclear spin of ^{13}C ($I = 1/2$) and the Zeeman interaction given by eq 8. Throughout the rest of this article, we will consider only the $^{13}C^{16}O$ isotope and hence will omit the isotope labels.

The largest splitting of the energy levels is due to the rotational structure, which gives rise to two manifolds of rotational states labeled $N = 0$ and 1 separated by 3.6761 cm^{-1}, approximately twice the rotational constant of CO. At zero magnetic field, the nuclear spin−rotation interaction splits all $N \geq 1$ energy levels into doublets with $j = N - 1/2$, $N + 1/2$, where $j = |\mathbf{N} + \mathbf{I}|$ is the total angular momentum of the molecule. Note that j is a good quantum number at a zero field. The splitting between the $j = 1/2$ and $j = 3/2$ levels in the $N = 1$ manifold is $(3/2)A$ or 2.4×10^{-6} cm^{-1}.

At high magnetic fields, the Zeeman interaction overcomes the hyperfine interaction, j is no longer conserved, and the energy levels approach the eigenstates of the Zeeman Hamiltonian (eq 8) $|NM_N\rangle|IM_I\rangle$ with the good quantum numbers N, M_N, and M_I indicated in Figure 1. In the $N = 0$ manifold, the nuclear spin−rotation interaction vanishes, and there are two Zeeman levels with $M_I = \pm 1/2$ as shown in the bottom panel of Figure 1. The $N = 1$ manifold contains six Zeeman levels $|N, M_N, M_I\rangle$ with $N = 1$, $M_N = -1$, 0, + 1, and $M_I = \pm 1/2$. To facilitate the following discussion, we will assign a state index (SI) to each Zeeman energy level, as shown in Figure 1 in order of increasing energy. It is worth noting that the states $|3\rangle$, $|4\rangle$, and $|5\rangle$ cross at $B \simeq 0.01$ T, where the nuclear spin−rotation interaction becomes comparable to the Zeeman interaction. The crossings are not avoided because the states have different values of m, the projection of j on the magnetic field axis, which is a good quantum number for a molecule in an external magnetic field.

3.2. Nuclear Spin Dynamics in Cold He−CO Collisions: Cross Sections and Rate Constants. We begin by considering the transitions between the two lowest nuclear spin levels of CO, $|N = 0, M_I = \pm 1/2\rangle$ induced by cold collisions with He atoms. Figure 2 shows the cross sections for transitions out of the ground ($|M_I = -1/2\rangle$) and the first excited ($|M_I = 1/2\rangle$) Zeeman levels labeled as 1 and 2 in Figure 1. The elastic cross sections $\sigma_{1\to1}$ and $\sigma_{2\to2}$ are on the order of $100-10^4$ Å^2 between 10 and 10 K, as is typical for cold atom−molecule collisions. The inelastic cross sections for nuclear spin-changing transitions within the $N = 0$ manifold $|M_I = 1/2\rangle \leftrightarrow |M_I = -1/2\rangle$ are extremely small, reaching values below 10^{-15} Å^2 at 10 mK.

Similarly to electron spin relaxation in collisions of $^2\Sigma$ molecules with atoms,[68,69] nuclear spin relaxation in cold atom−molecule collisions ($E < 2B_e$) proceeds indirectly via a three-step process. First, the molecule is temporarily excited to a closed-channel $N = 1$ state due to the coupling with the incident $N = 0$ channel induced by the anisotropy of the interaction potential. In the rotationally excited state, the nuclear spin is flipped by the nuclear spin−rotation interaction (eq 7). Finally, the molecule is de-excited to the ground $N = 0$ state through the interaction anisotropy coupling. Because the nuclear spin−rotation interaction is 2 to 3 orders of magnitude weaker than the electron spin−rotation interaction in $^2\Sigma$ molecules, nuclear spin relaxation will be suppressed by a factor of $\simeq(A/\gamma_{sr})^2$ (i.e., by an additional 4−6 orders of magnitude) compared to the electron spin relaxation mediated by the electron spin−rotation interaction $\gamma_{sr}\mathbf{N}\cdot\mathbf{S}$.[10,68]

At collision energies exceeding the rotational spacing ($E \geq 2B_e \simeq 5.3$ K for CO), $N = 0 \to 1$ rotational excitation

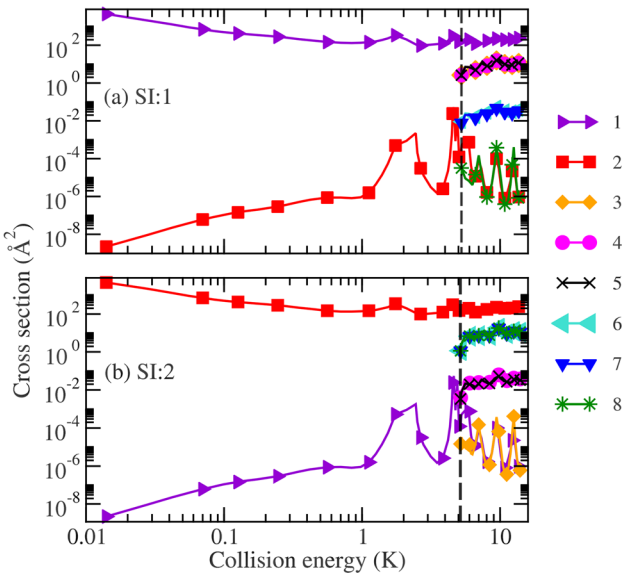

Figure 2. State-to-state cross sections for He + CO collisions for the initial Zeeman states in the $N = 0$ manifold: $|M_I = -1/2\rangle$ (a) and $|M_I = 1/2\rangle$ (b) in a magnetic field of 0.05 T plotted as a function of collision energy. The cross sections for the transitions $|1\rangle \to |2\rangle$, $|8\rangle$ and $|2\rangle \to |1\rangle$, $|3\rangle$ are multiplied by 10^6 for better visibility. Dashed lines indicate the energy gap between the $N = 0$ and $N = 1$ levels ($\simeq$5.3 K). The initial states are indicated in each panel. The various color-coded symbols indicate the final state indices (SIs) specified in Figure 1. The symbols do not represent the actual number of calculated points, which is 20 per order of magnitude (i.e., 20 points between 0.01 and 0.1 cm^{-1}, etc.).

transitions become energetically allowed, and the spin relaxation cross sections $\sigma_{2\to1}$ and $\sigma_{1\to2}$ increase dramatically. As in the case of electron spin relaxation,[10,14,68,70] this occurs because the $N = 0 \to 1$ transitions can now populate the open $N = 1$ states directly (rather than transiently).

The cross sections for nuclear spin-conserving rotational excitation increase slightly with collision energy as shown in Figure 2 and are the largest between spin-down energy levels $|1\rangle$ and $|3-5\rangle$ or between spin-up energy levels $|2\rangle$ and $|6-8\rangle$. On the other hand, the nuclear spin-flipping rotational excitation transitions $|1\rangle \to |6-8\rangle$ and $|2\rangle \to |3-5\rangle$ are suppressed by a factor of $\simeq$100. This is an example of a nuclear spin selection rule, discussed in more detail below. We observe several Feshbach resonances in the collision energy dependence of the cross sections $\sigma_{1\to2}$, $\sigma_{1\to8}$, $\sigma_{2\to1}$, and $\sigma_{2\to3}$ above 1 K.

In Figures 3 and 4, we show the cross sections for elastic scattering and rotational relaxation in He + CO collisions with CO molecules initially prepared in the different Zeeman sublevels of the $N = 1$ excited rotational state. For the fully spin-polarized initial states $|8\rangle$ and $|3\rangle$, we observe three groups of transitions, as shown in Figure 3. The dominant relaxation channels are $|8\rangle \to |2\rangle$ ($|1, 1, 1/2\rangle \to |0, 0, 1/2\rangle$), $|8\rangle \to |6\rangle$ ($|1, 1, 1/2\rangle \to |1, -1, 1/2\rangle$), and $|8\rangle \to |7\rangle$ ($|1, 1, 1/2\rangle \to |1, 0, 1/2\rangle$) (group I). All of these transitions conserve nuclear spin projection M_I but change either N or M_N. The second most probable are the nuclear spin-flipping transitions $|8\rangle \to |4\rangle$ ($|1, 1, 1/2\rangle \to |1, 0, -1/2\rangle$) and $|8\rangle \to |5\rangle$ ($|1, 1, 1/2\rangle \to |1, 1, -1/2\rangle$) (group II), which change M_I but conserve N. The cross sections in group II are $\simeq 10^3$ times smaller than those in group I. In turn, the least probable transitions from group III, $|8\rangle \to |1\rangle$ ($|1, 1, 1/2\rangle \to |0, 0, -1/2\rangle$) and $|8\rangle \to |3\rangle$

https://doi.org/10.1021/acs.jpca.2c08646
J. Phys. Chem. A 2023, 127, 4511−4525

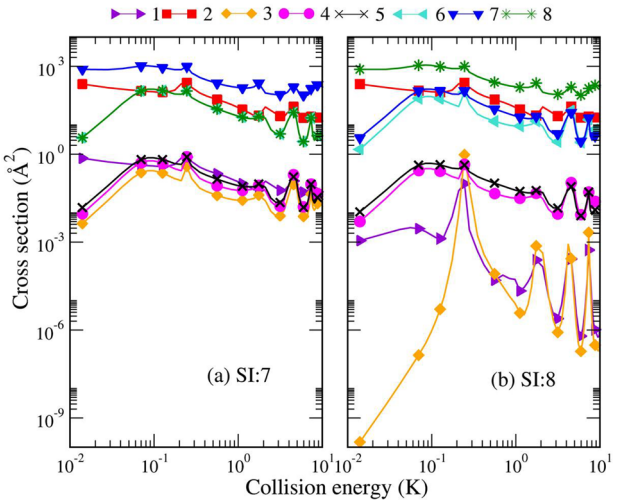

Figure 3. State-to-state cross sections of He + CO collisions for the initial Zeeman states $|7\rangle$ and $|8\rangle$ in the $N = 1$ manifold plotted as a function of collision energy. The initial states are indicated in each panel. The various color-coded symbols indicate the final state indices (SIs) specified in Figure 1. The cross sections for the transitions $|8\rangle \rightarrow |1\rangle$ and $|8\rangle \rightarrow |3\rangle$ are multiplied by 10^6 for better visibility. The symbols do not represent the actual number of calculated points, which is 20 per order of magnitude (i.e., 20 points between 0.01 and 0.1 cm^{-1}, etc.).

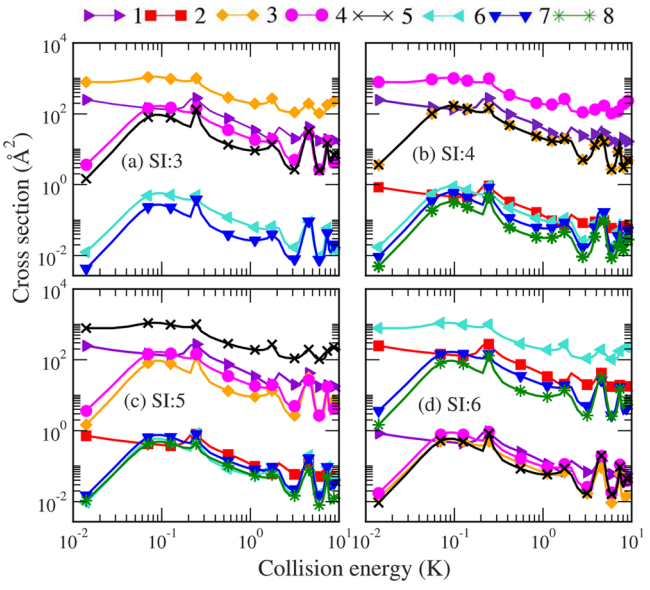

Figure 4. State-to-state cross sections of He + CO collisions for the initial Zeeman states $|3\rangle - |6\rangle$ in the $N = 1$ manifold plotted as a function of collision energy. The initial states are indicated in each panel. The various color-coded symbols indicate the final state indices (SIs) specified in Figure 1. The cross sections for group III transitions $|3\rangle \rightarrow |2\rangle$ and $|3\rangle \rightarrow |8\rangle$ are negligibly small and hence not shown in panel (a). The symbols do not represent the actual number of calculated points, which is 20 per order of magnitude (i.e., 20 points between 0.01 and 0.1 cm^{-1}, etc.).

$(|1, 1, 1/2\rangle \rightarrow |1, -1, -1/2\rangle)$, are further suppressed by a factor of $\simeq 10^3$ compared to group II transitions. The final states in group III are also fully spin-polarized, with a maximal difference between the initial and final values of M_N and M_I. This suppression is expected because the fully spin-polarized states do not experience the nuclear spin−rotation interaction and thus the matrix elements of the interaction potential connecting them are zero. The cross section for the $|8\rangle \rightarrow |3\rangle$ transition is extremely small at all collision energies as shown in Figure 3(b). Similar trends are observed for the fully spin-polarized initial state $|3\rangle$ as well as in our recent calculations on the electron spin relaxation of rotationally excited CaH molecules in cold collisions with He atoms in a magnetic field.[71]

For non-fully spin-polarized $N = 1$ initial states $|4\rangle - |6\rangle$ and $|7\rangle$ (see Figures 4 and 3), we observe two distinct groups of transitions, one of which (group I) has much larger cross sections than the other (group II). Group I transitions conserve M_I but change either M_N or N as in the fully polarized case considered above. Group II transitions are nuclear spin-flipping transitions that change M_I and/or M_N. There are no strongly suppressed group III transitions for the initial states $|4\rangle - |7\rangle$ since these initial states are not fully spin-polarized. We note that the nuclear spin-flipping transitions in group III are forbidden in the first Born approximation due to zero nuclear spin overlap between the initial and final states. These transitions occur due to higher-order couplings through intermediate rotationally excited states mediated by the anisotropy of the interaction potential (see above).[10,68]

The energy dependence of the cross sections shown in Figures 3 and 4 displays a number of resonances. Four substantial resonances occur in the cross sections for group III transitions, such as $|8\rangle \rightarrow |3\rangle$, $|1\rangle$ and $|3\rangle \rightarrow |8\rangle$, $|2\rangle$ at 0.25, 2, 4, and 7.2 K, respectively. We have verified that these resonances are Feshbach resonances, rather than shape resonances, by calculating the partial wave decomposition of the cross sections (eq 10) and finding that no single partial wave dominates at the resonance energies. The likely reason that Feshbach resonances are absent in the group I and, to a lesser extent, group II transitions is the large magnitude of the cross sections for these transitions, leading to an enhanced decay width of the resonances. As a result, the resonance peaks become suppressed.[72]

Typical temperatures used in ^{4}He buffer gas cooling experiments range from $\simeq$1 to 4 K and higher, so it is instructive to consider the thermally averaged collision rates. The temperature dependence of the elastic and inelastic collision rates is plotted in Figure 5. The resonances shown in Figure 2 are narrow compared with the width of the Maxwell−Boltzmann energy distribution. As a result, the resonances are washed away by thermal averaging and the calculated rate coefficients increase monotonously as a function of temperature between 1 and 5 K for the transitions of $|1\rangle \rightarrow |1\rangle$, $|2\rangle$ and $|2\rangle \rightarrow |1\rangle$, $|2\rangle$. We observe that the rate coefficients for the excitation transitions $|1\rangle$, $|2\rangle \rightarrow |3\rangle - |8\rangle$ shown in the lower panel of Figure 5 decay exponentially at lower temperatures and remain nearly constant at higher temperatures. This is because the rotationally excited final states become energetically closed at collision energies below 5.3 K, and their cross sections vanish, as shown in Figure 2.

Nevertheless, it should be noted that the rates for rotational excitation via the $|2\rangle \rightarrow |3\rangle - |8\rangle$ transitions are larger than those for the $|2\rangle \rightarrow |1\rangle$ transition by several orders of magnitude even at $T = 0.5$ K. This is due to the large magnitude of the excitation cross sections at the high-energy tail of the Maxwell−Boltzmann distribution above 5.3 K (see Figure 2), which makes a significant contribution to the thermal collision rates even though transitions to rotationally

https://doi.org/10.1021/acs.jpca.2c08646
J. Phys. Chem. A 2023, 127, 4511−4525

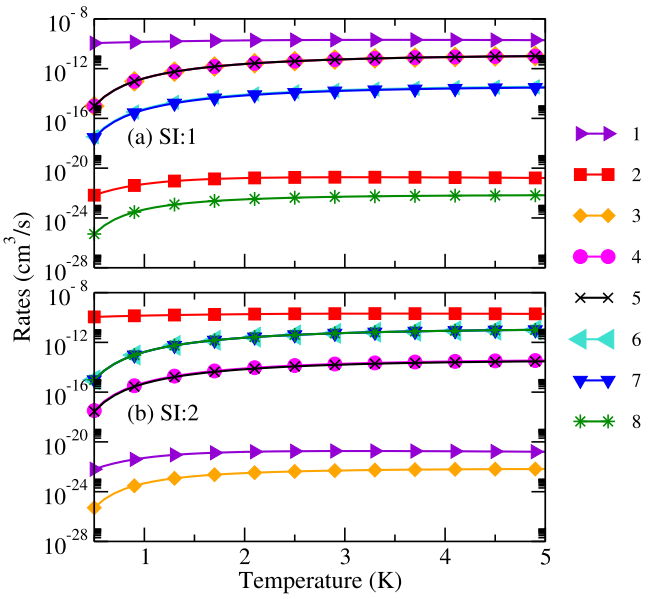

Figure 5. Thermally averaged rate coefficients for He + CO collisions plotted as a function of temperature for the initial hyperfine Zeeman states $|1\rangle$ and $|2\rangle$ of CO. The magnetic field is 0.05 T. The initial states are indicated in each panel. The various color-coded symbols indicate the final state indices (SIs) specified in Figure 1.

excited closed channels are energetically forbidden below 5.3 K. As shown below, this causes a steep temperature dependence of nuclear spin relaxation times of CO molecules immersed in a cold buffer gas of He.

The thermally averaged rate coefficients for the transitions out of the initial states in the $N = 1$ manifold are shown in Figure 6. As before, we observe that the rate coefficients are

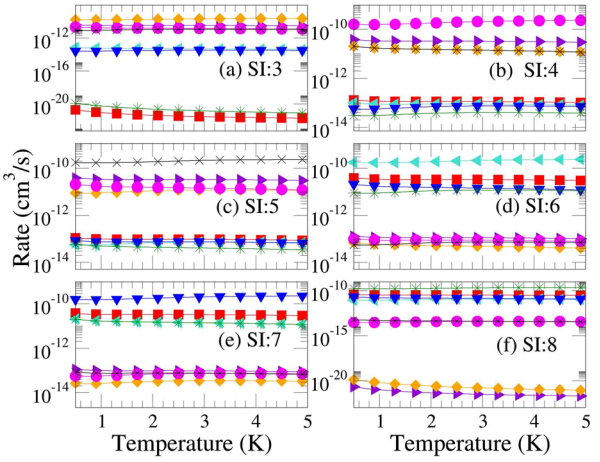

Figure 6. Thermally averaged rate coefficients for He + CO collisions for the rotationally excited initial states $|3\rangle - |8\rangle$ in a magnetic field of 0.05 T. The initial states are indicated in each panel. The various color-coded symbols indicate the final state indices (SIs) specified in Figure 1.

smooth functions of temperature, with the resonant structure present in the energy-dependent cross sections being washed away by thermal averaging. While all of the nuclear spin-conserving (group I) transitions have similar transition rates on the order of 10^{-11} cm^3/s, the rates of nuclear spin-flipping transitions (group II) are 3 orders of magnitude smaller.

The rates of group III transitions involving the fully spin-polarized initial and final states $|8\rangle$, $|3\rangle$, $|2\rangle$, and $|1\rangle$ are further suppressed compared to those of group II transitions by several orders of magnitude, reflecting the trend discussed above for the cross sections. As shown in Figure 6(a) and (f), the transition $|8\rangle \leftrightarrow |3\rangle$ is particularly strongly suppressed. This is because the initial and final states are fully spin-polarized, and hence they are not coupled by the spin−rotation interaction, just like the $|1\rangle$ and $|2\rangle$ states in the $N = 0$ manifold. This remarkable suppression of collisional transitions is similar to the electron and nuclear spin selection rules in spectroscopy ($\Delta S = 0$ and $\Delta I = 0$[73]). A similar suppression was observed for the transitions between the fully electron-spin-polarized $N = 1$ Zeeman states of CaH($^2\Sigma^+$) molecules in cold collisions with He atoms.[71]

The dominant relaxation and excitation pathways between the Zeeman sublevels of CO($N = 0$, 1) in cold collisions with He are summarized in Figure 7. The most prominent group I

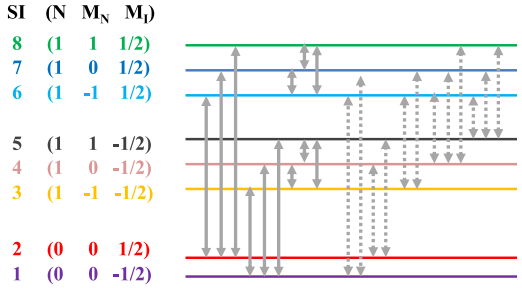

Figure 7. Schematic diagram of relaxation and excitation transitions among the eight lowest Zeeman levels of CO in cold collisions with He atoms. The most likely nuclear spin-conserving (group I) transitions are marked by solid arrows. Nuclear spin-flipping (group II) transitions are marked with dashed arrows. Group III transitions are forbidden and hence not shown.

transitions, indicated by solid arrows, conserve the nuclear spin projection. These transitions occur between spin-up Zeeman levels ($|2\rangle \leftrightarrow |6-8\rangle$, $|6\rangle \leftrightarrow |7\rangle$, $|7\rangle \leftrightarrow |8\rangle$ and $|6\rangle \leftrightarrow |8\rangle$) or between spin-down Zeeman levels ($|1\rangle \leftrightarrow |3-5\rangle$, $|3\rangle \leftrightarrow |4\rangle$, $|4\rangle \leftrightarrow |5\rangle$, and $|3\rangle \leftrightarrow |5\rangle$).

The next most efficient are the nuclear spin-flipping transitions from group II marked by dashed arrows in Figure 7. Such transitions include $|1\rangle \leftrightarrow |6-7\rangle$, $|2\rangle \leftrightarrow |4-5\rangle$, $|3\rangle \leftrightarrow |6-7\rangle$, and $|4-5\rangle \leftrightarrow |6-7\rangle$. The group III spin-flipping transitions involving the nuclear spin-stretched states $|1\rangle$, $|2\rangle$, $|3\rangle$, and $|8\rangle$ have extremely small rate coefficients. These forbidden transitions are not shown in Figure 7.

3.3. Magnetic Field Dependence.

In this section, we consider the magnetic field dependence of the state-to-state He + CO cross sections. This dependence is depicted in Figure 8 (see also Appendix D) at $E = 0.014$, 0.251, and 2 K and the initial states $|7\rangle$ and $|8\rangle$. We note that at these energies, the cross sections for transitions between the $N = 0$ Zeeman states $|1\rangle$ and $|2\rangle$ (not shown in Figure 8) are field-independent.

For the fully spin-stretched initial state $|8\rangle$, we observe three groups of transitions as shown in panels a, c, and e of Figure 8, with group III transitions to the fully spin polarized states $|3\rangle$ and $|1\rangle$ having extremely small cross sections, which are independent of the magnetic field (see above). Transitions to the final states $|2\rangle$, $|7\rangle$, and $|6\rangle$ belong to group I. These transitions have large cross sections and display no dependence on the magnetic field because both the initial and final states

https://doi.org/10.1021/acs.jpca.2c08646
J. Phys. Chem. A 2023, 127, 4511−4525

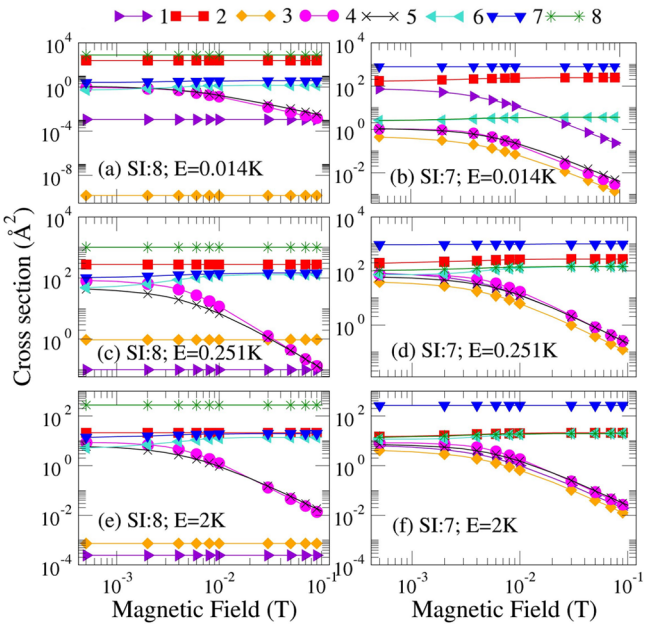

Figure 8. Magnetic field dependence of state-to-state cross sections for $^{13}C^{16}O-^{4}He$ collisions. The collision energy and initial state index are indicated in each panel. The cross sections $\sigma_{8\to1}$ and $\sigma_{8\to3}$ are multiplied by 10^6 to aid visibility. The various color-coded symbols indicate the final state indices (SIs) specified in Figure 1.

have the same nuclear spin projections. These transitions are similar to purely rotational transitions, which conserve the nuclear spin.

$$H = \begin{pmatrix} 2B_e + B_0\mu_I(g_I M_I + g_N M_N) + AM_N M_I & A\sqrt{2 - M_N(M_N+1)}\sqrt{3/4 - M_I(M_I-1)} \\ A\sqrt{2 - M_N'(M_N'-1)}\sqrt{3/4 - M_I'(M_I'+1)} & 2B_e + B_0\mu_I(g_I M_I' + g_N M_N') + AM_N' M_I' \end{pmatrix} \quad (14)$$

The diagonal matrix elements are composed of the rotational, Zeeman, and spin−rotation contributions, whereas the off-diagonal elements are due to the spin−rotation interaction.

To be specific, we chose to examine the magnetic field dependence of eigenstates $|5\rangle$ and $|7\rangle$ composed of the basis states $|1, 0, 1/2\rangle$ and $|1, 1, -1/2\rangle$. In the basis of these states the matrix (eq 14) takes the form (in units of cm^{-1})

$$H = \begin{pmatrix} 3.675940 + B(0.0001785) & 8.209 \times 10^{-7} \\ 8.209 \times 10^{-7} & 3.67594056 + B(-0.0001126) \end{pmatrix} \quad (15)$$

At low magnetic fields, the diagonal matrix elements are nearly degenerate, and hence the uncoupled basis states are strongly mixed by the off-diagonal spin−rotation interaction terms. As the field increases, the degeneracy is lifted, and the eigenstates of the Hamiltonian become progressively closer to the bare uncoupled states $|1, M_N, M_I\rangle$.

We can see this more directly by looking at the eigenvectors of our model 2 × 2 Hamiltonian (eq 14)

Importantly, group II transitions $|8\rangle \to |4\rangle$ and $|8\rangle \to |5\rangle$ show a pronounced magnetic field dependence. These transitions change the nuclear spin projection, and the final states are superpositions of basis states $|NM_NM_I\rangle$ with different M_N and M_I mixed by the nuclear spin−rotation interaction.

In Figure 8(b), (d), and (f), we observe similar trends in the magnetic field dependence of the transitions originating from the initial state $|7\rangle$, except that there are no group III transitions as state $|7\rangle$ is not fully spin-polarized. As many as four transitions out of this state display a marked magnetic field dependence, and the final states populated by these transitions ($|1\rangle$, $|3\rangle$, $|4\rangle$, and $|5\rangle$) have the opposite nuclear spin projection to the initial state, state $|7\rangle$.

The magnetic field dependence can be explained by examining the initial and final Zeeman states involved in these group II transitions. At any finite magnetic field and $N > 0$, M_N and M_I are generally not good quantum numbers because of the nuclear spin−rotation interaction mixing. The molecular eigenstates $|4\rangle$, $|5\rangle$, $|6\rangle$, and $|7\rangle$ can be written as a superposition of two uncoupled basis states $|N, M_N, M_I\rangle$

$$|\gamma\rangle = c_{\gamma;1}|N = 1, M_N, M_I\rangle + c_{\gamma;2}|N = 1, M_N', M_I'\rangle \quad (13)$$

To obtain the mixing coefficients consider the representation of the molecular Hamiltonian (eq 3) in the basis $\{|1, M_N, M_I\rangle, |1, M_N', M_I'\rangle\}$

$$|7\rangle = \cos(\theta/2)|1, 0, 1/2\rangle + \sin(\theta/2)|1, 1, -1/2\rangle$$
$$|5\rangle = -\sin(\theta/2)|1, 0, 1/2\rangle + \cos(\theta/2)|1, 1, -1/2\rangle$$
$$\tan\theta = \left(\frac{\sqrt{2}\gamma}{B\mu(g_N - g_I) + \frac{\gamma}{2}}\right) \quad (16)$$

where the amplitudes $\cos\left(\frac{\theta}{2}\right)$ and $\sin\left(\frac{\theta}{2}\right)$ approximate the coefficients $c_{\gamma;1}$ and $c_{\gamma;2}$ in eq 13. In the strong magnetic field limit, the argument $x = \sqrt{2}\gamma/\left(B\mu(g_N - g_I) + \frac{\gamma}{2}\right)$ is small. Replacing $\tan(x) \to x$, we obtain $\theta \simeq C/B$, where $C = \sqrt{2}\gamma/\mu(g_N - g_I)$.

In the inset of Figure 9, we plot the eigenvector components of the eigenstate $|5\rangle$ vs the magnetic field. We see that as the field increases, the spin-up component of state $|5\rangle$ decreases and the eigenstate approaches the bare state $|1, 1, -1/2\rangle$. This numerical result agrees with eq 16, which predicts $|5\rangle \to |1, 1, -1/2\rangle$ at large B, where $\theta \simeq C/B \to 0$.

Having discussed the magnetic field dependence of the Zeeman states, we can now calculate the inelastic cross sections between these states in the first Born approximation (here and throughout this work, we use atomic units, where $\hbar = 1$)

https://doi.org/10.1021/acs.jpca.2c08646
J. Phys. Chem. A 2023, 127, 4511−4525

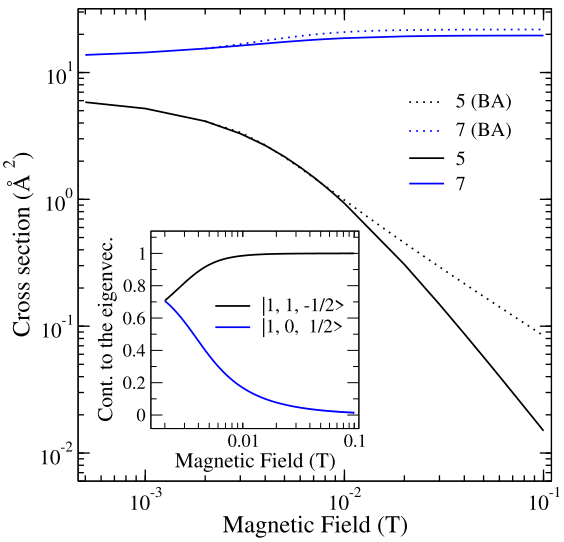

Figure 9. Magnetic field dependence of He + CO state-to-state cross sections for the initial state $|8\rangle$ and final states $|5\rangle$ and $|7\rangle$ at a collision energy of 2 K. Solid lines are cross sections calculated using the accurate CC method. Dashed lines represent results obtained in the Born approximation (BA). The inset shows the contribution of the basis states $|N, M_N, M_I\rangle$ to state $|5\rangle$ as a function of the magnetic field.

$$\sigma_{i\to j}^{B} = \frac{\mu^2}{4\pi^2}\left|\int e^{i\mathbf{q}\cdot\mathbf{R}} V_{ij}(\mathbf{R}) d^3R\right|^2 \tag{17}$$

where $\mathbf{q}$ is the transferred momentum and $V_{ij}(\mathbf{R})$ is the matrix element of the interaction potential between the eigenstates $|i\rangle$ and $|j\rangle$. Expanding our initial and final states in the bare state basis $|N, M_N, M_I\rangle$ defined above

$$\begin{aligned} |i\rangle &= c_{i1}|1, M_{N_i}, 1/2\rangle + c_{i2}|1, M'_{N_i}, -1/2\rangle \\ |j\rangle &= c_{j1}|1, M_{N_j}, 1/2\rangle + c_{j2}|1, M_{N_j}{}', -1/2\rangle. \end{aligned} \tag{18}$$

the cross sections in the Born approximation (eq 17) can be written as

$$\begin{aligned} \sigma_{i\to j}^{B} = \frac{\mu^2}{4\pi^2}\Bigg| \int e^{i\mathbf{q}\cdot\mathbf{R}} (& c_{i1}c_{j1}\langle 1, M_{N_j}, 1/2|V|1, M_{N_i}, 1/2\rangle \\ &+ c_{i1}c_{j2}\langle 1, M_{N_j}{}', -1/2|V|1, M_{N_i}, 1/2\rangle \\ &+ c_{j1}c_{i2}\langle 1, M_{N_j}, 1/2|V|1, M'_{N_i}, -1/2\rangle \\ &+ c_{i2}c_{j2}\langle 1, M_{N_j}{}', -1/2|V|1, M'_{N_i}, -1/2\rangle)\, d^3R\Bigg|^2 \end{aligned} \tag{19}$$

The atom−molecule interaction PES is independent of the nuclear spin and hence diagonal in M_I. We can thus rewrite eq 19 as

$$\begin{aligned} \sigma_{i\to j} = \frac{\mu^2}{4\pi^2}\Bigg| \int e^{i\mathbf{q}\cdot\mathbf{R}} (& c_{i1}c_{j1}\langle 1, M_{N_j}, 1/2|V|1, M_{N_i}, 1/2\rangle \\ &+ c_{i2}c_{j2}\langle 1, M_{N_j}{}', -1/2|V|1, M'_{N_i}, -1/2\rangle)\, d^3R\Bigg|^2 \end{aligned} \tag{20}$$

For simplicity, we will consider the case of the fully spin-polarized initial Zeeman state such as $|8\rangle$, where $c_{i2} = 0$, and eq 20 simplifies to

$$\begin{aligned} \sigma_{8\to 7} &= \frac{\mu^2}{4\pi^2}\cos^2(\theta/2)\left|\int e^{i\mathbf{q}\cdot\mathbf{R}}\langle 1, 1, 1/2|V|1, 0, 1/2\rangle\, d^3R\right|^2 \\ \sigma_{8\to 5} &= \frac{\mu^2}{4\pi^2}\sin^2(\theta/2)\left|\int e^{i\mathbf{q}\cdot\mathbf{R}}\langle 1, 1, 1/2|V|1, 0, 1/2\rangle\, d^3R\right|^2 \end{aligned} \tag{21}$$

where $\sigma_{8\to 7}$ is the cross section for the nuclear spin-conserving transition $|8\rangle \to |7\rangle$ and $\sigma_{8\to 5}$ is the cross section for the nuclear spin-flipping transition $|8\rangle \to |5\rangle$. The prefactors $\cos^2(\theta/2)$ and $\sin^2(\theta/2)$ give the magnetic field scalings of the inelastic cross sections.

The cross sections calculated using eq 21 are compared with the accurate CC calculations in Figure 9. The cross section $\sigma_{8\to 5}$ decreases with an increasing magnetic field. This trend is qualitatively reproduced by the Born approximation, which makes clear that the decline of the cross section $\sigma_{8\to 5}$ is caused by the decreasing mixing between the different nuclear spin components of the eigenstate $|5\rangle$ in eq 21. As stated above, the mixing angle scales as $\theta \simeq B^{-1}$ in the large B-field limit and thus $\sigma_{8\to 5} \simeq B^{-2}$.

In contrast, the cross section for the $|8\rangle \to |7\rangle$ transition tends to a constant value in the high B-field limit due to the mixing coefficient $\cos^2(\theta/2)$ in eq 21 approaching unity as $\theta \to 0$. At higher fields, the cross sections computed in the Born approximation start to deviate from the accurate CC results. This could be a consequence of multichannel effects, which become more pronounced as the cross sections become smaller at higher B fields. The Born approximation does, however, capture the overall trend in the magnetic field dependence of scattering cross sections observed in accurate CC calculations.

3.4. Nuclear Spin Relaxation Dynamics of CO Molecules Immersed in a Cold He Buffer Gas. In this section, we examine the relaxation dynamics of CO molecules prepared in a single $N = 0$ nuclear spin sublevel in cold collisions with He atoms. To this end, we use the standard rate equations,[74−76] which describe the time evolution of populations of the individual molecular eigenstates $|m\rangle$

$$\dot{\rho}_{mm}(t) = \sum_{n\neq m}\rho_{nn}(t)W_{mn} - \rho_{mm}(t)\sum_{n\neq m}W_{nm} \tag{22}$$

where $W_{mn} = K_{n\to m}n_{\mathrm{He}}$ are the rates for the transitions $|n\rangle \to |m\rangle$ induced by collisions with helium atoms, n_{He} is the atomic density (we assume that $n_{\mathrm{He}} \gg n_{\mathrm{CO}}$), and $\rho_{nn}(t)$ is the diagonal density matrix element (the population of state $|n\rangle$) at time t. The He + CO bimolecular transition rates are obtained from rigorous CC calculations, as described above, and we take $n_{\mathrm{He}} = 10^{14}$ cm^{-3}.

Figure 10 shows the time evolution of populations of the lowest nuclear spin states of CO molecules initially prepared in the pure nuclear spin state $|2\rangle$. These results are obtained by solving the rate eq 22 numerically using a basis set including the eight lowest hyperfine states of CO (see Figure 1). The population of the initial state $|2\rangle$ relaxes to equilibrium due to collisions with buffer gas atoms. The equilibrium state is given by the Boltzmann distribution $\rho_{ij}^{\mathrm{eq}} = \delta_{ij}e^{-E_i/k_BT}/Z$, where Z is the partition function. At $T \ll 2B_e/k_B$, only the $N = 0$ nuclear spin sublevels are thermally populated. The energy gap between the

https://doi.org/10.1021/acs.jpca.2c08646
J. Phys. Chem. A 2023, 127, 4511−4525

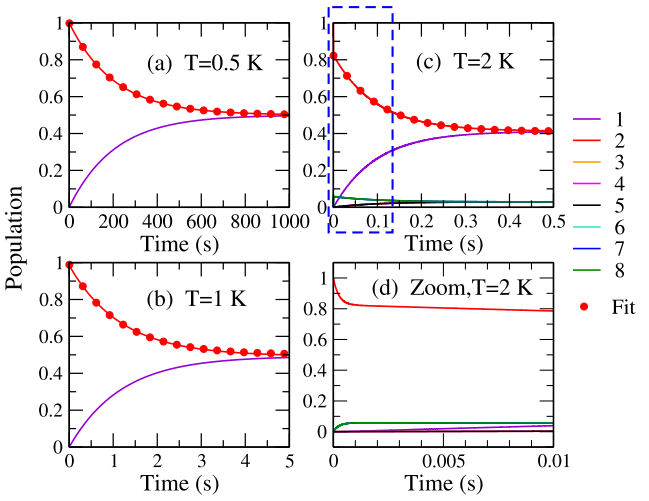

Figure 10. Time dynamics of CO nuclear spin state populations in cold collisions with He atoms at different temperatures: (a) $T = 0.5$ K, (b) $T = 1$ K, and (c) $T = 2$ K, respectively. Panel (d) shows details of short-time dynamics at $T = 2$ K. The red dots denote the exponential fit (see the text).

$N = 0$ nuclear spin sublevels of CO is extremely small compared to k_BT at $T \geq 1$ mK and $B < 0.1$ T (see Figure 1), so we expect $\rho_{11}^{eq} = \rho_{22}^{eq} \simeq 1/2$ as is indeed observed in Figure 10(a) and (b). At $T = 2$ K, a small fraction of the overall population (<10%) ends up in $N = 1$ rotational states as this temperature is no longer negligibly small compared to the rotational spacing between the $N = 0$ and $N = 1$ levels (5.3 K).

The relaxation time scale is strongly temperature-dependent. At $T = 0.5$ K, the relaxation is extremely slow, and thermal equilibrium is reached only on the time scale of hundreds of seconds. At higher temperatures, the relaxation occurs much faster, taking ≃0.1 s at 2 K. Table 1 lists the nuclear spin relaxation times of CO molecules obtained by fitting the time dynamics of state populations in Figure 10 to an exponential form $\rho_{22}(t) = \frac{1}{2}(1 + e^{-t/T_1})$.

Table 1. Nuclear Spin Relaxation Times of CO Molecules in the Nuclear Spin State $|2\rangle$ ($|N = 0, M_I = 1/2\rangle$) in Collisions with He Atoms[a]

$T(K)$	0.5	1.0	2.0
T_1(s)	205	1.12	0.098

[a]The magnetic field is 0.05 T.

The drastic increase in the relaxation time of state $|2\rangle$ at lower temperatures can be explained by the extremely small transition rates for the nuclear-spin-changing transitions $|2\rangle \leftrightarrow |1\rangle$ (see Figure 5), which lead to equilibration of the nuclear spin degrees of freedom. The opposite trend is observed at higher temperatures, where the relaxation times decrease dramatically due to the corresponding increase in the $|2\rangle \leftrightarrow |1\rangle$ transition rates.

We finally note that the nuclear spin relaxation times of CO molecules are moderately sensitive to the interaction PES (to within a factor of 2), as shown in Appendix A.

4. SUMMARY AND CONCLUSIONS

We developed a rigorous CC methodology for quantum nuclear spin dynamics in cold, weakly anisotropic collisions between $^1\Sigma^+$ molecules and structureless atoms in the presence of an external magnetic field. As in all CC methods, the solution of the time-independent Schrödinger equation is expanded in a channel basis set. Here, we use a basis set composed of direct products of rotational and nuclear spin basis functions of the diatomic molecule. The theory is conceptually similar to the one developed previously for electron spin depolarization in cold atom−molecule collisions[9,10] in which the electron spin basis functions are replaced by their nuclear spin counterparts. Nonetheless, our calculations show that nuclear spin relaxation occurs much more slowly than electron spin relaxation due to the much weaker interactions of nuclear spins with the rotational degrees of freedom.

We apply our methodology to study transitions between the different nuclear spin sublevels of $^{13}C^{16}O$ in cold collisions with ^{4}He buffer atoms. This system is experimentally relevant as buffer-gas-cooled diatomic and polyatomic molecules have been probed spectroscopically in a number of recent experiments.[25−34] We perform rigorous coupled-channel quantum scattering calculations based on an accurate *ab initio* potential energy surface of He-CO, focusing on transitions between the nuclear spin sublevels of the ground ($N = 0$) and the first excited ($N = 1$) rotational states.

Our calculations show that state-to-state transitions between the nuclear spin sublevels of polar molecules (such as CO) in cold collisions with buffer-gas atoms (such as He) are governed by several selection rules. The transition probability depends on (i) whether the nuclear spin projection of the initial state changes in a collision and (ii) whether the initial and final states are fully spin-polarized. The dominant transitions that belong to group I conserve nuclear spin projection M_I but change either N or M_N. Group II transitions, which change M_I and occur between nonfully polarized initial and/or final Zeeman states, are 3 orders of magnitude slower. Finally, the weakest group III transitions change M_I and occur between the fully polarized initial and final Zeeman states. This hierarchy of transitions is expected: on the basis of the weakness of the nuclear spin−rotation coupling between the different Zeeman levels, one could predict that the strongest transitions would be those that conserve M_I. In addition, similar propensity rules for electron spin-rotational transitions were found in our previous work on cold ^{4}He + ^{40}CaH collisions.[71] However, because the Zeeman levels are coupled in a nontrivial way by the anisotropy of the atom−molecule interaction potential, only rigorous quantum scattering calculations can provide quantitative insight into the hierarchy of transitions.

We find that only group II transitions have a marked magnetic field dependence. The origin of this dependence is the field-induced mixing between the different spin-rotational basis functions that compose the initial and final molecular eigenstates. Specifically, as the magnetic field increases, the eigenstates become more polarized; i.e., they acquire a definite value of the nuclear spin projection M_I. Because the atom−molecule interaction potential is diagonal in M_I, both the initial and final states must have the same value of M_I for the transition to occur in the first order. As a result, the cross sections for group II transitions originating from the fully spin-polarized eigenstates are proportional to the overlap between the nuclear spin components of the initial and final states. This overlap is most strongly field-dependent when the initial and final states have magnetic g factors of the opposite sign, such as

https://doi.org/10.1021/acs.jpca.2c08646
J. Phys. Chem. A 2023, 127, 4511−4525

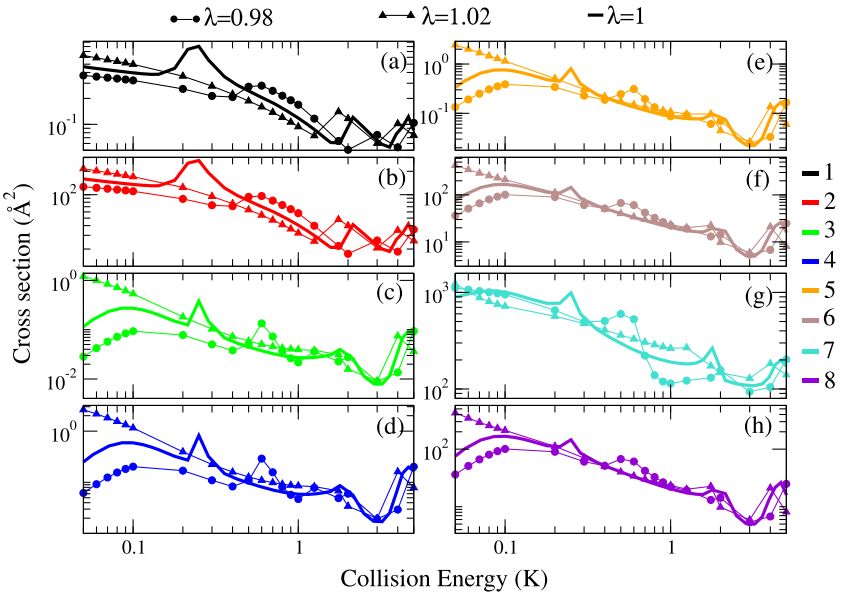

Figure 11. State-to-state cross sections for He + CO collisions from the initial state $|7\rangle$ as a function of collision energy. Each panel represents a different final state starting from $|1\rangle$ and ending with $|8\rangle$. The magnetic field is 0.05 T.

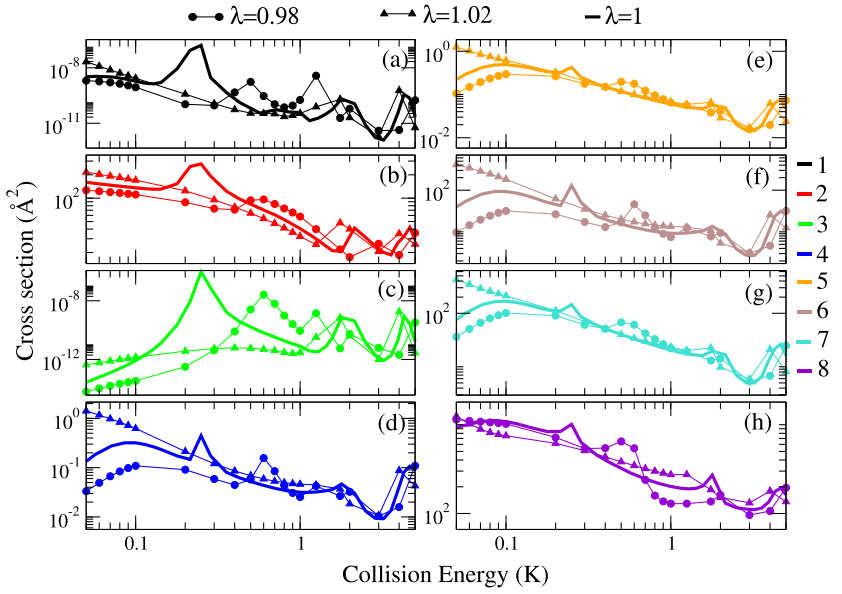

Figure 12. State-to-state cross sections for He + CO collisions from the initial state $|8\rangle$ as a function of collision energy. Each panel represents a different final state starting from $|1\rangle$ and ending with $|8\rangle$. The magnetic field is 0.05 T.

states $|8\rangle$ and $|5\rangle$ in Figure 1. In this case, the overlap scales as $1/B$, and the inelastic cross section scales as $1/B^2$.

In contrast, for group I transitions the nuclear spin overlap factor depends on the magnetic field only weakly since both the initial and final states have the same M_I values. For group III transitions, the nuclear spin overlap is zero at all magnetic fields and transitions occur through an indirect mechanism involving field-independent couplings to rotationally excited states. We observe a number of Feshbach resonances in the collision energy dependence of the integral cross sections, which are particularly pronounced for group III transitions.

Finally, we explored the time dynamics of nuclear spin relaxation of CO molecules immersed in a cold gas of He atoms using rate equation simulations based on the CC collision rates computed in this work. While the relaxation times of the $N = 0$ nuclear spin sublevels are extremely long at very low temperatures ($T \ll 2B_e/k_B$), they decline sharply with increasing temperature due to a dramatic increase in the nuclear spin-flipping rates. Our simulations thus indicate that preparing long-lived nuclear spin sublevels of diatomic molecules in inert buffer gases would require cooling the molecules to temperatures much lower than the spacing between the $N = 0$ and $N = 1$ rotational states.

Because spin-flipping transitions in the $N = 0$ manifold belong to group III (and hence, their cross sections are extremely small), extremely long relaxation times might be expected. However, the precise values of collision rates responsible for the nuclear spin relaxation time scales cannot be determined without performing the rigorous quantum scattering calculations reported here.

https://doi.org/10.1021/acs.jpca.2c08646
J. Phys. Chem. A 2023, 127, 4511−4525

APPENDIX A: SENSITIVITY TO THE INTERACTION POTENTIAL

In this section, we explore the sensitivity of ^{4}He + ^{13}C^{16}O collision cross sections, rate constants, and relaxation times to small changes in the interaction potential. This is necessary because low-temperature scattering observables are known to be strongly affected by such changes,[4,20] and the accuracy of *ab initio* interaction potentials, such as the He-CO potential used in this work, is limited. To vary the interaction potential, we multiply it by a constant scaling factor λ as done in previous theoretical work.[20] As the He-CO scattering calculations are computationally intensive, we choose two values of the scaling parameter, λ = 1.02 and 0.98, to explore the range of uncertainty in the He-CO interaction potential of ±2%.

Figures 11 and 12 show the cross sections for the initial states $|7\rangle$ and $|8\rangle$ to all final states calculated for the unscaled (λ = 1) and scaled interaction potentials. We observe that altering the potential changes the background values of scattering cross sections and shifts the positions of scattering resonances. This is expected as the scaling changes the positions of the last bound states of the He-CO collision complex, which are responsible for Feshbach resonances. The changes are particularly pronounced in the s-wave regime below 0.1 K.

Table 2 lists the state-to-state He-CO collision rates calculated with unscaled (λ = 1) and scaled (λ = 0.98, 1.02) interaction PESs. While the largest rates do not change significantly upon PES scaling, the smaller rates that correspond to group II and III transitions are more sensitive to the PES. The most sensitive are group III transitions, whose rates are the smallest and are most affected by scattering resonances.

Table 2. State-to-State He + CO Collision Rates Calculated for the Unscaled PES (Last Column) and Scaled PESs (First and Second Columns)[a]

transition	+2%	−2%	unchanged
$\|1\rangle \rightarrow \|2\rangle$	5.45×10^{-23}	3.26×10^{-24}	6.69×10^{-23}
$\|1\rangle \rightarrow \|8\rangle$	8.06×10^{-27}	1.23×10^{-26}	5.10×10^{-26}
$\|2\rangle \rightarrow \|1\rangle$	5.45×10^{-23}	3.27×10^{-24}	6.37×10^{-23}
$\|2\rangle \rightarrow \|3\rangle$	8.06×10^{-27}	1.24×10^{-26}	5.10×10^{-26}
$\|3\rangle \rightarrow \|2\rangle$	2.38×10^{-22}	3.65×10^{-22}	2.00×10^{-21}
$\|3\rangle \rightarrow \|8\rangle$	2.24×10^{-23}	1.66×10^{-21}	1.25×10^{-20}
$\|6\rangle \rightarrow \|3\rangle$	1.05×10^{-13}	9.01×10^{-14}	7.01×10^{-14}
$\|8\rangle \rightarrow \|1\rangle$	2.38×10^{-22}	3.64×10^{-22}	2.00×10^{-21}
$\|8\rangle \rightarrow \|2\rangle$	3.72×10^{-11}	3.95×10^{-11}	3.81×10^{-11}
$\|8\rangle \rightarrow \|3\rangle$	2.23×10^{-23}	1.66×10^{-21}	1.25×10^{-20}
$\|8\rangle \rightarrow \|6\rangle$	1.92×10^{-11}	9.97×10^{-12}	8.89×10^{-12}

[a]These transitions were calculated at 0.5 K. The magnetic field is 0.05 T.

Finally, we explore the sensitivity of nuclear spin relaxation dynamics to small changes in the He-CO interaction PES. Figure 13 shows the time evolution of the populations of the lowest nuclear spin states of CO initially prepared in the pure nuclear spin state $|2\rangle$ for unscaled (λ = 0) and scaled (λ = 0.98, 1.02) interaction potentials. We observe that although changing the interaction potential has an impact on the details of relaxation dynamics, the qualitative features of the dynamics are not affected. This is because the relaxation time scales are determined by many state-to-state transitions, and the overall effect of the interaction PES on these transition rates tends to average out. The nuclear spin relaxation times of CO molecules in a buffer gas of He listed in Table 3 are seen to change by a factor of 2 when the interaction PES is varied by ±2%.

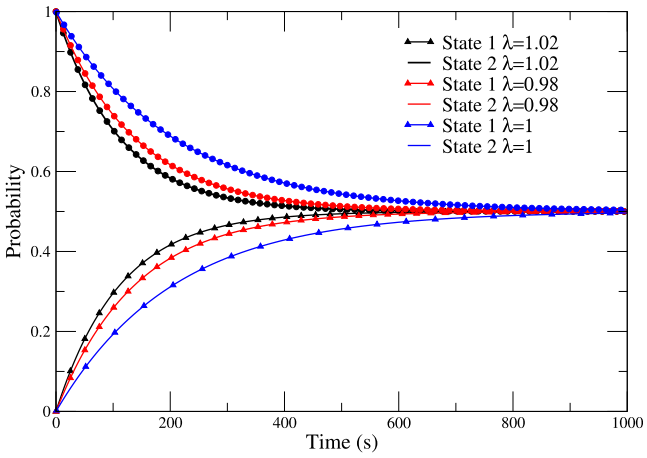

Figure 13. Time dynamics of the nuclear spin state populations of CO in cold collisions with He atoms at T = 0.5 K for the unscaled and scaled He−CO interaction potentials. The dots denote the exponential fits, which provide the T_1 times.

Table 3. Nuclear Spin Relaxation Times of CO Molecules in the Nuclear Spin State $|2\rangle$ ($|N = 0, M_I = 1/2\rangle$) in Collisions with He Atoms at T = 0.5 K[a]

PES type	unscaled	λ = 1.02	λ = 0.98
T_1(s)	205	111	137

[a]The magnetic field is 0.05 T.

APPENDIX B: COMPARISON WITH PREVIOUS HE + CO CALCULATIONS

To test our newly developed quantum scattering code, we calculated the cross sections for rotational relaxation in ^{4}He + ^{12}C^{16}O collisions as a function of collision energy. The results are compared in Figure 14 with the reference calculations performed by Balakrishnan et al.[58] and by Yang et al.[61] Note that the ^{12}C^{16}O isotope lacks the nuclear spin, so these calculations do not account for it. In order to compare with the previous results computed using a total angular momentum basis,[58,61] we averaged our M_N-resolved cross sections over the three degenerate M_N components of the N = 1 initial state.

As shown in Figure 14, our cross sections are in good agreement with the reference values at collision energies above 1 cm^{-1}. In particular, the positions and widths of five scattering resonances, which occur between 1 and 10 cm^{-1}, agree closely. We observe a significant discrepancy at the lowest-energy resonance at E = 0.7 cm^{-1} and in the s-wave threshold regime, where our results are above the reference values. We attribute these discrepancies to small differences in the rotational constants of CO, and in the reduced masses of He-CO used in the present and the previous[58,61] calculations. It is well established that such small differences can have a large effect on scattering observables at ultralow temperatures.[4,20]

APPENDIX C: PES SCALING

Here, we describe the scaling of the He-CO PES, which is necessary to account for the shift of the center of mass of ^{13}CO

https://doi.org/10.1021/acs.jpca.2c08646
J. Phys. Chem. A 2023, 127, 4511−4525

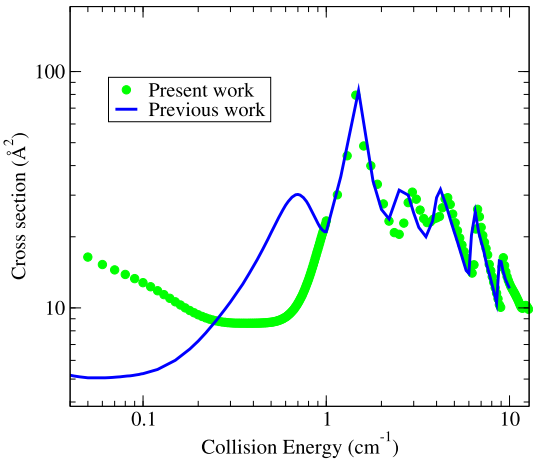

Figure 14. Collision energy dependence of the inelastic cross section for the $N = 1 \rightarrow 0$ transition in ^{4}He + ^{12}C^{16}O collisions calculated using the present code (green/gray dots). The results of independent quantum scattering calculations[58,61] are shown as the solid blue (gray) line.

compared to ^{12}CO. To this end, we follow the procedure described in ref 77. The transformation between the He−^{13}C^{16}O Jacobi coordinates (R, r, θ) and the He−^{12}C^{16}O Jacobi coordinates (R', r', θ') is given by (assuming $r = r'$)

$$R = R'\sqrt{1 + (\Delta/R')^2 - 2\Delta/(R' \cos\theta')}$$

$$\theta = \arccos\left(\frac{R' \cos\theta' - \Delta}{R}\right) \tag{23}$$

where Δ is the shift of the center-of-mass position between ^{13}C^{16}O and ^{12}C^{16}O.

APPENDIX D: MAGNETIC FIELD DEPENDENCE OF HE + CO CROSS SECTIONS FOR THE INITIAL STATES |3⟩, |4⟩, |5⟩, AND |6⟩

The magnetic field dependence of the cross sections for the initial states |1⟩, |2⟩, |7⟩, and |8⟩ is discussed in the main text (section 3.3). Here, we present additional results for the initial states |3⟩, |4⟩, |5⟩, and |6⟩ (Figures 15 and 16).

In Figure 15(b), (d), and (f), we observe three groups of transitions for the fully spin-stretched initial state |3⟩ in the $N = 1$ manifold. As discussed in the main text, nuclear spin-conserving (group I) transitions to the final states |1⟩, |4⟩, and |5⟩ are magnetic field-independent. The nuclear spin-flipping transitions involving the fully spin-polarized final states |2⟩ and |8⟩ belong to group III and have the smallest cross sections, which also show no magnetic field dependence. Only group II transitions have a significant magnetic field dependence.

The initial state |4⟩ is not fully spin-polarized, so transitions out of this state can belong to either group I or group II. In panels (a), (c), and (e) of Figure 15, we show the cross sections for these transitions. As before, nuclear spin-conserving transitions to final states |1⟩, |3⟩, and |5⟩ (group I transitions) are independent of the magnetic field. In contrast, nuclear spin-flipping transitions from group II populating final states |2⟩, |6⟩, |7⟩, and |8⟩ display a strong magnetic field dependence.

Figure 16 shows the cross sections for the initial states |5⟩ and |6⟩. We observe very similar trends to those discussed above for the initial states |3⟩ and |4⟩. The transitions can be

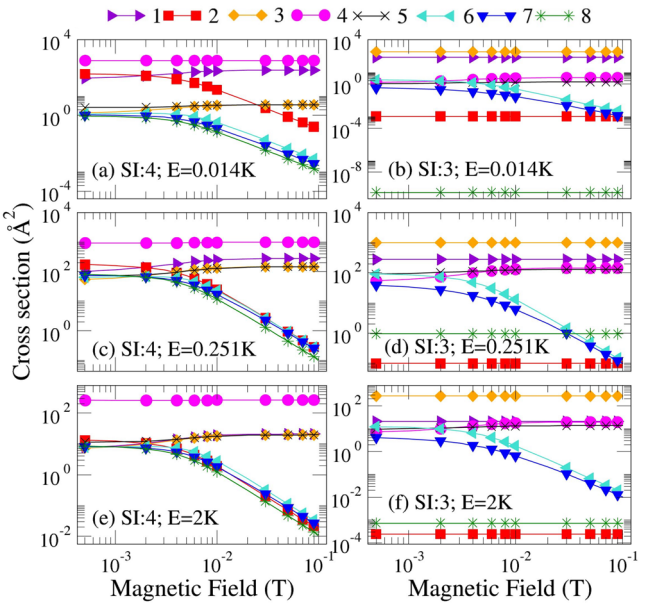

Figure 15. Magnetic field dependence of state-to-state cross sections for ^{4}He + ^{13}C^{16}O collisions. The collision energy and the initial state index are indicated in each panel. The cross sections $\sigma_{3\rightarrow2}$ and $\sigma_{3\rightarrow8}$ are multiplied by 10^6 to aid visibility. The various color-coded symbols indicate the final state indices (SIs) specified in Figure 1.

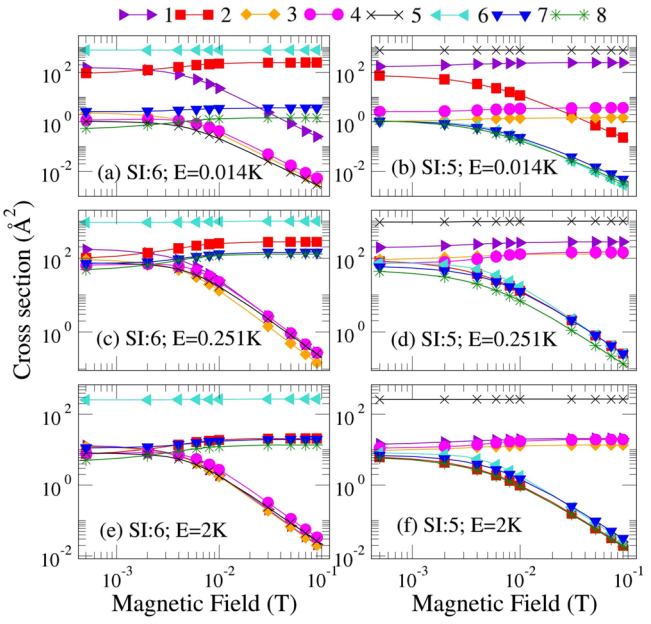

Figure 16. Magnetic field dependence of state-to-state cross sections for ^{4}He + ^{13}C^{16}O collisions. The collision energy and the initial state index are indicated in each panel. The various color-coded symbols indicate the final state indices (SIs) specified in Figure 1.

classified in two groups: group I (|5⟩ → |1⟩, |3⟩, |4⟩; |6⟩ → |2⟩, |7⟩, |8⟩) and group II (|5⟩ → |2⟩, |6⟩, |7⟩, |8⟩; |6⟩ → |1⟩, |3⟩, |4⟩, |5⟩).

AUTHOR INFORMATION

Corresponding Author

Timur V. Tscherbul − *Department of Physics, University of Nevada, Reno, Nevada 89557, United States;* orcid.org/0000-0001-5689-040X; Email: ttscherbul@unr.edu

https://doi.org/10.1021/acs.jpca.2c08646
J. Phys. Chem. A 2023, 127, 4511−4525

Authors

Rebekah Hermsmeier − *Department of Physics, University of Nevada, Reno, Nevada 89557, United States;* orcid.org/0000-0002-2979-1649

Xiaodong Xing − *Department of Physics, University of Nevada, Reno, Nevada 89557, United States;* orcid.org/0000-0001-6933-7048

Complete contact information is available at: https://pubs.acs.org/10.1021/acs.jpca.2c08646

Notes

The authors declare no competing financial interest.

■ ACKNOWLEDGMENTS

We thank Jonathan Weinstein for stimulating discussions and Balakrishnan Naduvalath for providing the results of quantum dynamics calculations of cold ^{4}He + ^{12}C^{16}O collisions.[58,61] This work was supported by the NSF through the CAREER program (PHY-2045681).

■ REFERENCES

(1) Carr, L. D.; DeMille, D.; Krems, R. V.; Ye, J. Cold and ultracold molecules: science, technology and applications. *New J. Phys.* **2009**, *11*, 055049.

(2) Lemeshko, M.; Krems, R. V.; Doyle, J. M.; Kais, S. Manipulation of molecules with electromagnetic fields. *Mol. Phys.* **2013**, *111*, 1648−82.

(3) Krems, R. V. Cold Controlled Chemistry. *Phys. Chem. Chem. Phys.* **2008**, *10*, 4079−4092.

(4) Balakrishnan, N. Perspective: Ultracold molecules and the dawn of cold controlled chemistry. *J. Chem. Phys.* **2016**, *145*, 150901.

(5) Bohn, J. L.; Rey, A. M.; Ye, J. Cold molecules: Progress in quantum engineering of chemistry and quantum matter. *Science* **2017**, *357*, 1002−1010.

(6) Hutzler, N. R. Polyatomic molecules as quantum sensors for fundamental physics. *Quantum Sci. Technol.* **2020**, *5*, 044011.

(7) Lara, M.; Bohn, J. L.; Potter, D.; Soldán, P.; Hutson, J. M. Ultracold Rb-OH Collisions and Prospects for Sympathetic Cooling. *Phys. Rev. Lett.* **2006**, *97*, 183201.

(8) Tscherbul, T. V.; Kłos, J.; Buchachenko, A. A. Ultracold spin-polarized mixtures of $^2\Sigma$ molecules with S-state atoms: Collisional stability and implications for sympathetic cooling. *Phys. Rev. A* **2011**, *84*, 040701.

(9) Volpi, A.; Bohn, J. L. Magnetic-field effects in ultracold molecular collisions. *Phys. Rev. A* **2002**, *65*, 052712.

(10) Krems, R. V.; Dalgarno, A. Quantum-mechanical theory of atom-molecule and molecular collisions in a magnetic field: Spin depolarization. *J. Chem. Phys.* **2004**, *120*, 2296−2307.

(11) Weinstein, J.; deCarvalho, R.; Guillet, T.; Friedrich, B.; Doyle, J. M. Magnetic Trapping of Calcium Monohydride Molecules at Millikelvin Temperatures. *Nature* **1998**, *395*, 148−150.

(12) Campbell, W. C.; Tscherbul, T. V.; Lu, H.-I.; Tsikata, E.; Krems, R. V.; Doyle, J. M. Mechanism of Collisional Spin Relaxation in $^3\Sigma$ Molecules. *Phys. Rev. Lett.* **2009**, *102*, 013003.

(13) Hummon, M. T.; Tscherbul, T. V.; Kłos, J.; Lu, H.-I.; Tsikata, E.; Campbell, W. C.; Dalgarno, A.; Doyle, J. M. Cold N + NH Collisions in a Magnetic Trap. *Phys. Rev. Lett.* **2011**, *106*, 053201.

(14) Singh, V.; Hardman, K. S.; Lu, M.-J.; Ellis, A.; Morrison, M. J.; Weinstein, J. D. Inelastic collisions of CaH with He at cryogenic temperatures. *Mol. Phys.* **2013**, *111*, 1711−1715.

(15) Segev, Y.; Pitzer, M.; Karpov, M.; Akerman, N.; Narevicius, J.; Narevicius, E. Collisions between cold molecules in a superconducting magnetic trap. *Nature* **2019**, *572*, 189−193.

(16) Son, H.; Park, J. J.; Ketterle, W.; Jamison, A. O. Collisional cooling of ultracold molecules. *Nature* **2020**, *580*, 197−200.

(17) Jurgilas, S.; Chakraborty, A.; Rich, C. J. H.; Caldwell, L.; Williams, H. J.; Fitch, N. J.; Sauer, B. E.; Frye, M. D.; Hutson, J. M.; Tarbutt, M. R. Collisions between Ultracold Molecules and Atoms in a Magnetic Trap. *Phys. Rev. Lett.* **2021**, *126*, 153401.

(18) Suleimanov, Y. V.; Tscherbul, T. V.; Krems, R. V. Efficient method for quantum calculations of molecule-molecule scattering properties in a magnetic field. *J. Chem. Phys.* **2012**, *137*, 024103.

(19) Morita, M.; Kosicki, M. B.; Żuchowski, P. S.; Tscherbul, T. V. Atom-molecule collisions, spin relaxation, and sympathetic cooling in an ultracold spin-polarized Rb(^{2} S)−SrF($^2\Sigma^+$) mixture. *Phys. Rev. A* **2018**, *98*, 042702.

(20) Morita, M.; Krems, R. V.; Tscherbul, T. V. Universal Probability Distributions of Scattering Observables in Ultracold Molecular Collisions. *Phys. Rev. Lett.* **2019**, *123*, 013401.

(21) Tscherbul, T. V.; Krems, R. V. Tuning Bimolecular Chemical Reactions by Electric Fields. *Phys. Rev. Lett.* **2015**, *115*, 023201.

(22) Patterson, D.; Rasmussen, J.; Doyle, J. M. Intense atomic and molecular beams via neon buffer-gas cooling. *New J. Phys.* **2009**, *11*, 055018.

(23) Hutzler, N. R.; Lu, H.-I.; Doyle, J. M. The Buffer Gas Beam: An Intense, Cold, and Slow Source for Atoms and Molecules. *Chem. Rev.* **2012**, *112*, 4803−4827.

(24) Porterfield, J. P.; Satterthwaite, L.; Eibenberger, S.; Patterson, D.; McCarthy, M. C. High sensitivity microwave spectroscopy in a cryogenic buffer gas cell. *Rev. Sci. Instrum.* **2019**, *90*, 053104.

(25) Egorov, D.; Weinstein, J. D.; Patterson, D.; Friedrich, B.; Doyle, J. M. Spectroscopy of laser-ablated buffer-gas-cooled PbO at 4 K and the prospects for measuring the electric dipole moment of the electron. *Phys. Rev. A* **2001**, *63*, 030501.

(26) Lu, M.-J.; Weinstein, J. D. Cold TiO($X^3\Delta$)-He collisions. *New J. Phys.* **2009**, *11*, 055015.

(27) Patterson, D.; Schnell, M.; Doyle, J. M. Enantiomer-specific detection of chiral molecules via microwave spectroscopy. *Nature* **2013**, *497*, 475−477.

(28) Iwata, G. Z.; McNally, R. L.; Zelevinsky, T. High-resolution optical spectroscopy with a buffer-gas-cooled beam of BaH molecules. *Phys. Rev. A* **2017**, *96*, 022509.

(29) Changala, P. B.; Weichman, M. L.; Lee, K. F.; Fermann, M. E.; Ye, J. Rovibrational quantum state resolution of the C_{60} fullerene. *Science* **2019**, *363*, 49−54.

(30) Santamaria, L.; Di Sarno, V.; Aiello, R.; De Rosa, M.; Ricciardi, I.; De Natale, P.; Maddaloni, P. Infrared Comb Spectroscopy of Buffer-Gas-Cooled Molecules: Toward Absolute Frequency Metrology of Cold Acetylene. *Int. J. Mol. Sci.* **2021**, *22*, 250.

(31) Hofsäss, S.; Doppelbauer, M.; Wright, S. C.; Kray, S.; Sartakov, B. G.; Pérez-Ríos, J.; Meijer, G.; Truppe, S. Optical cycling of AlF molecules. *New J. Phys.* **2021**, *23*, 075001.

(32) Daniel, J. R.; Wang, C.; Rodriguez, K.; Hemmerling, B.; Lewis, T. N.; Bardeen, C.; Teplukhin, A.; Kendrick, B. K. Spectroscopy on the $A^1\Pi \leftarrow X^1\Sigma^+$ transition of buffer-gas-cooled AlCl. *Phys. Rev. A* **2021**, *104*, 012801.

(33) Liu, L. R.; Changala, P. B.; Weichman, M. L.; Liang, Q.; Toscano, J.; Kłos, J.; Kotochigova, S.; Nesbitt, D. J.; Ye, J. Collision-Induced C_{60} Rovibrational Relaxation Probed by State-Resolved Nonlinear Spectroscopy. *PRX Quantum* **2022**, *3*, 030332.

(34) Bu, W.; Zhang, Y.; Liang, Q.; Chen, T.; Yan, B. Saturated absorption spectroscopy of buffer-gas-cooled Barium monofluoride molecules. *Front. Phys.* **2022**, *17*, 62502.

(35) Walker, T. G.; Happer, W. Spin-exchange optical pumping of noble-gas nuclei. *Rev. Mod. Phys.* **1997**, *69*, 629−642.

(36) Gentile, T. R.; Nacher, P. J.; Saam, B.; Walker, T. G. Optically polarized ^{3}He. *Rev. Mod. Phys.* **2017**, *89*, 045004.

(37) Barskiy, D. A.; et al. NMR Hyperpolarization Techniques of Gases. *Chem.—Eur. J.* **2017**, *23*, 725−751.

(38) Spiliotis, A. K.; Xygkis, M.; Koutrakis, M. E.; Tazes, K.; Boulogiannis, G. K.; Kannis, C. S.; Katsoprinakis, G. E.; Sofikitis, D.; Rakitzis, T. P. Ultrahigh-density spin-polarized hydrogen isotopes from the photodissociation of hydrogen halides: new applications for

laser-ion acceleration, magnetometry, and polarized nuclear fusion. *Light Sci. Appl.* **2021**, *10*, 35.
(39) Park, J. W.; Yan, Z. Z.; Loh, H.; Will, S. A.; Zwierlein, M. W. Second-scale nuclear spin coherence time of ultracold $^{23}Na^{40}K$ molecules. *Science* **2017**, *357*, 372−375.
(40) Gregory, P. D.; Blackmore, J. A.; Bromley, S. L.; Hutson, J. M.; Cornish, S. L. Robust storage qubits in ultracold polar molecules. *Nat. Phys.* **2021**, *17*, 1149−1153.
(41) Ospelkaus, S.; Ni, K.-K.; Wang, D.; de Miranda, M. H. G.; Neyenhuis, B.; Quéméner, G.; Julienne, P. S.; Bohn, J. L.; Jin, D. S.; Ye, J. Quantum-State Controlled Chemical Reactions of Ultracold KRb Molecules. *Science* **2010**, *327*, 853−857.
(42) Ni, K.-K.; Ospelkaus, S.; Wang, D.; Quéméner, G.; Neyenhuis, B.; de Miranda, M. H. G.; Bohn, J. L.; Ye, J.; Jin, D. S. Dipolar collisions of polar molecules in the quantum regime. *Nature (London)* **2010**, *464*, 1324−1328.
(43) Simbotin, I.; Côté, R. Effect of nuclear spin symmetry in cold and ultracold reactions: D + para/ortho-H_2. *New J. Phys.* **2015**, *17*, 065003.
(44) Tscherbul, T. V.; Grinev, T. A.; Yu, H.-G.; Dalgarno, A.; Kłos, J.; Ma, L.; Alexander, M. H. Cold collisions of polyatomic molecular radicals with S-state atoms in a magnetic field: An ab initio study of He + $CH_2(\tilde{X})$ collisions. *J. Chem. Phys.* **2012**, *137*, 104302.
(45) Kilaj, A.; Gao, H.; Rösch, D.; Rivero, U.; Küpper, J.; Willitsch, S. Observation of different reactivities of para and ortho-water towards trapped diazenylium ions. *Nat. Commun.* **2018**, *9*, 2096.
(46) Oka, T. Nuclear spin selection rules in chemical reactions by angular momentum algebra. *J. Mol. Spectrosc.* **2004**, *228*, 635−639.
(47) Hu, M.-G.; Liu, Y.; Nichols, M. A.; Zhu, L.; Quéméner, G.; Dulieu, O.; Ni, K.-K. Nuclear spin conservation enables state-to-state control of ultracold molecular reactions. *Nat. Chem.* **2021**, *13*, 435−440.
(48) Lara, M.; Bohn, J. L.; Potter, D. E.; Soldán, P.; Hutson, J. M. Cold collisions between OH and Rb: The field-free case. *Phys. Rev. A* **2007**, *75*, 012704.
(49) Tscherbul, T. V.; Kłos, J.; Rajchel, L.; Krems, R. V. Fine and hyperfine interactions in cold YbF-He collisions in electromagnetic fields. *Phys. Rev. A* **2007**, *75*, 033416.
(50) González-Martínez, M. L.; Hutson, J. M. Effect of hyperfine interactions on ultracold molecular collisions: $NH(^3\Sigma^-)$ with $Mg(^1S)$ in magnetic fields. *Phys. Rev. A* **2011**, *84*, 052706.
(51) Tscherbul, T. V.; Kłos, J. Magnetic tuning of ultracold barrierless chemical reactions. *Phys. Rev. Research* **2020**, *2*, 013117.
(52) Hermsmeier, R.; Kłos, J.; Kotochigova, S.; Tscherbul, T. V. Quantum Spin State Selectivity and Magnetic Tuning of Ultracold Chemical Reactions of Triplet Alkali-Metal Dimers with Alkali-Metal Atoms. *Phys. Rev. Lett.* **2021**, *127*, 103402.
(53) Chin, C.; Grimm, R.; Julienne, P.; Tiesinga, E. Feshbach resonances in ultracold gases. *Rev. Mod. Phys.* **2010**, *82*, 1225−1286.
(54) Quéméner, G.; Hu, M.-G.; Liu, Y.; Nichols, M. A.; Zhu, L.; Ni, K.-K. Model for nuclear spin product-state distributions of ultracold chemical reactions in magnetic fields. *Phys. Rev. A* **2021**, *104*, 052817.
(55) Wallis, A. O. G.; Krems, R. V. Magnetic Feshbach resonances in collisions of nonmagnetic closed-shell $^1\Sigma$ molecules. *Phys. Rev. A* **2014**, *89*, 032716.
(56) Brown, J.; Carrington, A. *Rotational Spectroscopy of Diatomic Molecules*; Cambridge University Press, 2003.
(57) Meerts, W.; De Leeuw, F.; Dymanus, A. Electric and magnetic properties of carbon monoxide by molecular-beam electric-resonance spectroscopy. *Chem. Phys.* **1977**, *22*, 319−324.
(58) Balakrishnan, N.; Dalgarno, A.; Forrey, R. C. Vibrational relaxation of CO by collisions with ^{4}He at ultracold temperatures. *J. Chem. Phys.* **2000**, *113*, 621−627.
(59) Zare, R. N. *Angular Momentum*; Wiley: New York, 1988.
(60) Johnson, B. R. The multichannel Log-Derivative Method for Scattering Calculations. *J. Comput. Phys.* **1973**, *13*, 445.
(61) Yang, B.; Stancil, P. C.; Balakrishnan, N.; Forrey, R. C. Close-coupling study of rotational energy transfer of CO (v = 2) by collisions with He atoms. *J. Chem. Phys.* **2005**, *123*, 134326.
(62) Klapper, G.; Lewen, F.; Gendriesch, R.; Belov, S.; Winnewisser, G. Sub-Doppler measurements of the rotational spectrum of $^{13}C^{16}O$. *J. Mol. Spectrosc.* **2000**, *201*, 124−127.
(63) Stoll, S.; Schweiger, A. EasySpin, a comprehensive software package for spectral simulation and anaylsis in EPR. *J. Magn. Reson.* **2006**, *178*, 42−55.
(64) Manolopoulos, D. E. An improved log derivative method for inelastic scattering. *J. Chem. Phys.* **1986**, *85*, 6425.
(65) Heijmen, T. G.; Moszynski, R.; Wormer, P. E.; Van Der Avoird, A. A new He-CO interaction energy surface with vibrational coordinate dependence. I. Ab initio potential and infrared spectrum. *J. Chem. Phys.* **1997**, *107*, 9921−9928.
(66) Moszynski, R.; Korona, T.; Wormer, P. E.; van der Avoird, A. Ab initio potential energy surface, infrared spectrum, and second virial coefficient of the He-CO complex. *J. Chem. Phys.* **1995**, *103*, 321−332.
(67) Bergeat, A.; Onvlee, J.; Naulin, C.; van der Avoird, A.; Costes, M. Quantum dynamical resonances in low-energy CO(j = 0) + He inelastic collisions. *Nat. Chem.* **2015**, *7*, 349−353.
(68) Krems, R. V.; Dalgarno, A.; Balakrishnan, N.; Groenenboom, G. C. Spin-flipping transitions in $^2\Sigma$ molecules induced by collisions with structureless atoms. *Phys. Rev. A* **2003**, *67*, 060703.
(69) Krems, R. V.; Groenenboom, G. C.; Dalgarno, A. Electronic Interaction Anisotropy between Atoms in Arbitrary Angular Momentum States. *J. Phys. Chem. A* **2004**, *108*, 8941−8948.
(70) Maussang, K.; Egorov, D.; Helton, J. S.; Nguyen, S. V.; Doyle, J. M. Zeeman Relaxation of CaF in Low-Temperature Collisions with Helium. *Phys. Rev. Lett.* **2005**, *94*, 123002.
(71) Koyu, S.; Hermsmeier, R.; Tscherbul, T. V. Total angular momentum representation for state-to-state quantum scattering of cold molecules in a magnetic field. *J. Chem. Phys.* **2022**, *156*, 034112.
(72) Hutson, J. M. Feshbach resonances in ultracold atomic and molecular collisions: threshold behaviour and suppression of poles in scattering lengths. *New J. Phys.* **2007**, *9*, 152.
(73) Jacobs, P. *Group Theory with Applications in Chemical Physics*; Cambridge University Press: Cambridge, U.K., 2005.
(74) Ramakrishna, S.; Seideman, T. Intense Laser Alignment in Dissipative Media as a Route to Solvent Dynamics. *Phys. Rev. Lett.* **2005**, *95*, 113001.
(75) Ramakrishna, S.; Seideman, T. Dissipative dynamics of laser induced nonadiabatic molecular alignment. *J. Chem. Phys.* **2006**, *124*, 034101.
(76) Blum, K. *Density Matrix Theory and Applications*; Springer Science & Business Media: New York, 2012.
(77) Żuchowski, P. S.; Hutson, J. M. Low-energy collisions of NH_3 and ND_3 with ultracold Rb atoms. *Phys. Rev. A* **2009**, *79*, 062708.

https://doi.org/10.1021/acs.jpca.2c08646
J. Phys. Chem. A 2023, 127, 4511−4525